REPUBLIC OF TURKEY

ADANA ALPARSLAN TÜRKEŞ SCIENCE AND TECHNOLOGY UNIVERSITY

GRADUATE SCHOOL OF NATURAL AND APPLIED SCIENCES

DEPARTMENT OF ELECTRICAL AND ELECTRONIC ENGINEERING

ELECTROCHEMICAL PRODUCTION OF TRANSITION METAL-BASED ELECTROCATALYSTS FOR WATER SPLITTING

EREN ERGEN

MASTER OF SCIENCE

ADANA 2022

REPUBLIC OF TURKEY

ADANA ALPARSLAN TÜRKEŞ SCIENCE AND TECHNOLOGY UNIVERSITY

GRADUATE SCHOOL OF NATURAL AND APPLIED SCIENCES

DEPARTMENT OF ELECTRICAL AND ELECTRONIC ENGINEERING

ELECTROCHEMICAL PRODUCTION OF TRANSITION METAL-BASED ELECTROCATALYSTS FOR WATER SPLITTING

EREN ERGEN

MASTER OF SCIENCE

SUPERVISOR

Assoc. Prof. Dr. BAŞAK DOĞRU MERT

ADANA 2022

I hereby declare that all information in this thesis has been obtained and presented in accordance with academic rules and ethical conduct. I also declare that, as required by these rules and conduct, I have fully cited and referenced all information that is not original to this work.

[Signature]

Eren ERGEN

ABSTRACT

ELECTROCHEMICAL PRODUCTION OF TRANSITION METAL-BASED ELECTROCATALYSTS FOR WATER SPLITTING

Eren ERGEN
Department of Electrical Electronic Engineering
Supervisor: Assoc. Prof. Dr. Başak DOĞRU MERT
Co-Supervisor: Assoc. Prof. Dr. Tuğçe DEMİRDELEN
January 2022, 85 pages

Due to increasing world population, technological developments and industrial activities, energy resources are decreasing day by day. In particular, the use of non-renewable energy resources (coal, oil, natural gas, etc.) seriously damages the world with effects such as greenhouse gas and global warming. Countries that see these negative effects on the world have started to explore renewable energy sectors in order to ensure the sustainability of energy and humanity in order to leave a prosperous living space for future generations. For this purpose; electrochemical hydrogen production by renewable sources assisted electrolysis may be a viable solution. For this reason, renewable energy sources are very important for the future of the world and also Turkey. Turkey imports many non-renewable energy resources such as oil and natural gas. Unfortunately, imported energy resources seriously affect Turkey's economy. The geographical location of our country is very suitable for renewable energy production, and it is in a very efficient position especially in terms of geothermal, solar and wind energy. We can raise the economy level of our country by investing in renewable energies. In this context, zero carbon emissions, high energy potential and "hydrogen energy", which have recently attracted the attention of researchers, draw attention. Although many methods are used to obtain hydrogen gas, alkaline electrolysis method is preferred due to its advantages. Electrode selection is very important in this method. As it is known, materials containing platinum (Pt) are used as the most efficient electrocatalysts due to the low overvoltages and high current densities of Pt based materials. However, the high cost of Pt greatly restricts its usage.

In this study, hydrogen gas was produced by utilizing the electrical energy produced from the wind turbine. During the production, the combination of various electrodes in the anode and cathode positions were observed in the experimental environment and the most convenient electrolysis cell for hydrogen gas production was determined. Platinum (Pt), stainless steel (SS), graphite (G), and copper (Cu) electrodes were used as anodes in the alkaline electrolysis cell. Graphite, was preferred as the cathode electrode due to its high electrical conductivity, low cost and corrosion resistance (in case of power cut). In addition, the G electrode was modified with nickel (Ni), cobalt (Co) and copper (Cu) by galvanostatic method. The ternary coating thickness was approximately 10 µm. The electrode surface was characterized by scanning electron microscopy and energy dispersive X-ray spectroscopy. The alkaline electrolysis process was carried out with two electrode systems for 15 minutes, the volumes of hydrogen gas ($H_{2(g)}$) produced for various potentials were determined. According to the experimental results, at each 3 V for 15 minutes of electrolysis time, the produced $H_{2(g)}$ various were; 15 mL; 11.13 mL; 9.30 mL; 8.71 mL; 13.12 mL; 10.10 mL; 10.97 mL for Pt-G (Cell-1), SS-G (Cell-2), G-G (Cell-3), Cu-G (Cell-4), SS-G/NiCoCu (Cell-5), GG/NiCoCu (Cell-6), Cu-G/NiCoCu (Cell-7), respectively.

Keywords: renewable energy, alkaline electrolysis, hydrogen gas production

ÖZET

SUYUN AYRIŞMASI İÇİN GEÇİŞ METAL TABANLI ELEKTROKATALİZÖRLERİN ELEKTROKİMYASAL ÜRETİMİ

Eren ERGEN
Elektrik Elektronik Mühendisliği Anabilim Dalı
Danışman: Doç. Dr. Başak DOĞRU MERT
İkinci Danışman: Doç. Dr. Tuğçe DEMİRDELEN
Ocak 2022, 85 sayfa

Dünya nüfusunun, teknolojik gelişmelerin ve endüstriyel faaliyetlerin giderek artmasından dolayı enerji kaynakları gün geçtikçe azalmaktadır. Özellikle, yenilenemeyen enerji kaynaklarının (kömür, petrol, doğal gaz, vb.) kullanımı sera gazı, küresel ısınma gibi etkilerle dünyaya ciddi derecede zarar vermektedir. Dünya üzerindeki bu olumsuz etkileri gören ülkeler, gelecek nesillere refah bir yaşam alanı bırakmak için enerjinin ve insanlığın sürdürülebilirliğini sağlamak adına yenilenebilir enerji sektörlerini keşfetmeye başlamışlardır. Bu amaca yönelik; yenilenebilir kaynaklar destekli elektroliz yoluyla elektrokimyasal hidrojen üretimi uygun bir çözüm olabilir. Bu sebeple, yenilenebilir enerji kaynakları, dünyanın ve Türkiye'nin geleceği için çok önemlidir. Türkiye petrol ve kömür gibi birçok yenilenemeyen enerji kaynağını ithal etmektedir. Ne yazık ki ithal edilen enerji kaynakları Türkiye'nin ekonomisini ciddi şekilde etkilemektedir. Ülkemizin coğrafi konumu yenilenebilir enerji üretimine çok uygun olup, özellikle jeotermal, güneş ve rüzgar enerjisi açısından oldukça verimli bir konumdadır. Yenilenebilir enerjilere yatırım yaparak ülkemizin ekonomi seviyesini daha yukarıya taşıyabiliriz. Bu bağlamda sıfır karbon emisyonu, yüksek enerji potansiyeli ve son dönemlerde araştırmacıların ciddi şekilde ilgisini toplamış olan "hidrojen enerjisi" dikkat çekmektedir. Hidrojen gazı eldesi için birçok yöntem kullanılmasına rağmen avantajları sebebiyle alkali elektroliz yöntemi tercih edilmektedir. Bu yöntemde elektrot seçimi çok önemlidir. Bilindiği üzere, platin (Pt) esaslı malzemelerin düşük aşırı gerilimleri ve yüksek akım yoğunlukları nedeniyle en verimli elektrokatalizörler olarak Pt ihtiva eden malzemeler kullanılmaktadır. Fakat Pt'nin maliyetinin yüksek olması, kullanımını ciddi oranda kısıtlamaktadır.

Bu çalışmada rüzgar türbininden üretilen elektrik enerjisinden faydanılarak hidrojen gazı üretilmiştir. Üretim sırasında çeşitli elektrotların anot ve katot pozisyonlarındaki kombinasyonu deneysel ortamda gözlemlenip hidrojen gazı üretimi için en uygun elektroliz hücresi tespit edilmiştir. Platin (Pt), paslanmaz çelik (SS), grafit (G), ve bakır (Cu) elektrotlar, alkali elektroliz hücresinde anot olarak kullanılmıştır. Grafit ise yüksek elektrik iletkenliği, düşük maliyeti ve korozyon direncinden (elektrik kesintisi durumunda) dolayı katot elektrotu olarak tercih edilmiştir. Ayrıca grafit elektrot, galvanostatik yöntemle nikel (Ni), kobalt (Co) ve bakır (Cu) ile modifiye edilmiştir. Üçlü kaplama kalınlığı yaklaşık 10 µm dir. Elektrot yüzeyi, taramalı elektron mikroskobu ve enerji dağılımlı X-ışını spektroskopisi ile karakterize edilmiştir. Alkali elektroliz işlemi, 15 dakika boyunca iki elektrot sistemi ile gerçekleştirilmiştir, çeşitli potansiyeller için üretilen hidrojen gazı (H_2(g)) hacimleri belirlenmiştir. Deneysel çalışmaların sonucuna göre; Pt-G (Hücre-1), SS-G (Hücre-2), G-G (Hücre-3), Cu-G (Hücre-4), SS-G/NiCoCu (Hücre-5), G-G/NiCoCu (Hücre-6), Cu-G/NiCoCu (Hücre-7) 'nin 3 V'da 15 dakika sonundaki hidrojen gazı üretimleri sırasıyla 15 mL; 11,13 mL; 9,30 mL; 8,71 mL; 13,12 mL; 10,10 mL; 10,97 mL dir.

Anahtar Kelimeler: yenilenebilir enerji, alkali elektroliz, hidrojen gazı üretimi

Dedication

I would like to dedicate my thesis to our martyrs and my dear father Hayati ERGEN

TABLE OF CONTENTS

LIST OF FIGURES

LIST OF TABLES

NOMENCLATURE

kWh	: Kilowatt Hour
W	: Watt
kW	: Kilowatt
MW	: Megawatt
GW	: Gigawatt
V	: Volt
A	: Amper
g	: Gram
kg	: Kilogram
m	: Meter
m^2	: Meter Square
cm	: Centimeter
cm^2	: Centimeter Square
L	: Liter
mL	: Milliliter
%	: Percent
s	: Second
I	: Current
E_d	: Decomposition Voltage
I_d	: Current Density
E_{over}	: Over Voltage
m	: Mass
G	: Graphite
G/Ni	: Nickel coated graphite
G/NiCo	: Nickel cobalt coated graphite
G/NiCoCu	: Nickel cobalt copper coated graphite
Zn	: Zinc
Pt	: Platinum
O_2	: Oxygen

H_2	: Hydrogen
N	: Nitrogen
CO_2	: Carbon Dioxide
CH_4	: Methane
KOH	: Potassium Hydroxide
Cl_2	: Chlorine
Cu	: Copper
S	: Sulfur
M	: Molarity
H_2SO_4	: Sulfuric Acid
e^-	: Electron
DC	: Direct Current
AC	: Alternating Current
Q	: Total Charge
V_t	: Theoretical Hydrogen Volumes
V_e	: Experimental Hydrogen Volumes
SEM	: Scanning Electron Microscope
EDX	: Energy-Dispersive X-Ray Spectroscopy
PMSG	: Permanent Magnet Synchronous Generator

1. INTRODUCTION

From the beginning of humanity to the period we are in, we humans always need energy. This energy, which we use to meet our needs or in the development of technology, unfortunately has a certain limit. Demand for energy is increasing day by day due to the increasing population rate of our world. For centuries, humanity has used oil, coal, wood, fossil fuels, in short, non-renewable energy sources to meet the increasing demands. Later, humanity realized that energy resources were being used unconsciously, and therefore harmful chemicals began to spread into the atmosphere and the environment. Unless we foresee the negative reflections and impact of non-renewable energy sources on the environment, it will be too late to compensate for side effects and we will steal the right to life of the next generation. In order to maintain the long-term viability of energy and mankind, we humans have begun to investigate renewable energy sources in a variety of ways. The consumption of renewable and sustainable energy to meet the needs will both reduce the risk level we are in and minimize the damage we cause to the environment. Therefore, renewable energy sources are significant for the world's and Turkey's futures. Turkey is a country that relies heavily on foreign countries to supply its energy requirements. Many energy sources, such as oil and coal, are imported. We harm both the ecology and the economy of our country by relying on nonrenewable resources. Renewable energy sources can help us escape our country's narrow economy and contribute significantly to our admission into a larger economy in this regard. We can use the financial investments we spend on energy resources imported from abroad for ourselves. We can develop more by using these investments for our own country. In addition, perhaps we can become a self-sufficient country by moving out of the position of a foreign-dependent country. Our country's physical-geographical location is ideal for renewable energy generation, and it is particularly productive in terms of geothermal, solar, and wind energy. Very serious work must be done in these areas for the development of Turkey. It appears to be an important way out to reduce energy imports. Because we can both increase our level of development and reduce the costs of serious investments we spend on energy. Renewable and sustainable energy sources are very important in this respect.

1.1. Energy classification

Renewable and non-renewable energy sources are categorised based on their generation. Coal, oil, natural gas, and nuclear energy are examples of non-renewable resources. Solar energy, hydroelectric energy, hydrogen energy, geothermal energy, sea-wave energy, biomass energy, and wind energy are examples of renewable resources. Renewable energy sources and non-renewable energy sources were examined.

1.1.1. Non-Renewable Energy Resources

Non-renewable energy sources are energy sources that have no continuity, are single-use and will eventually be depleted. Coal, oil, natural gas, nuclear energy can be cited as examples of non-renewable energy sources.

1.1.1.1. Coal

Coal is a sedimentary rock made up of plant-based organic compounds and inorganic components that has been generated over millions of years by exposing plant and wood remnants deposited in swamps to chemical and physical processes. Coal was first used by the Chinese. With the development of industrial and industrial areas, the use of coal has become widespread.

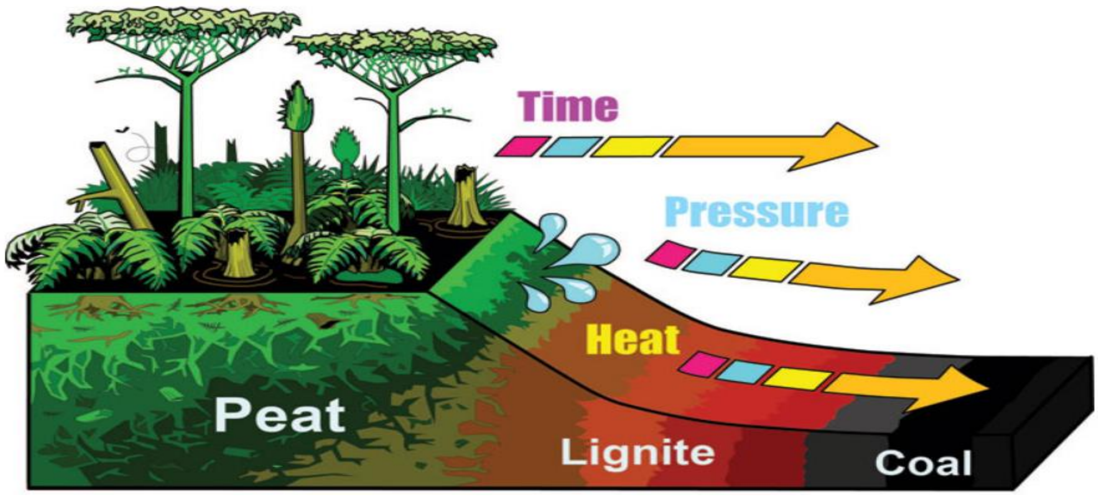

Figure 1.1. Formation stages of coal varieties

There are three types of coal;

- Anthracite
- Stone coal
- Lignite

Anthracite: Anthracite, the most expensive variety of coal, is made up of 95% carbon and has a high hardness and durability. For this reason, it is very difficult to burn anthracite, but when it is burned, more energy is generated than other coals.

Lignite: Lignite coals are usually soft, easily breakable and have a matte appearance that is not glossy. It is the least harmful type of coal in terms of Health and is often used in the production of electric power.

Stone coal: It is a type of coal that releases high energy when burned. The carbonization process is more than lignite and less than anthracite. Therefore, there is a medium level of charring process. The carbon ratio varies between 75-90%.

1.1.1.2. Oil

Oil is the greasy layer where the plant and animal remains in the seas decay under certain heat-pressure with the help of microorganisms. Oil, one of the most important resources in the world, has been the cause of many wars that took place in the past. Oil has various uses. The extracted crude oil is used as gasoline, kerosene, jet fuel, diesel fuel, heavy oils, and products such as asphalt, kerosene, lpg, paraffin and tar can be obtained from oil. As a result of the studies carried out, since the sulfur content of the petroleum is below 0.5%, the oil is regarded as sulfur-free.
The United States opened the world's first oil well in the state of Pennsylvania in 1859, producing the world's first regular oil, and the first production of 175 barrels of oil at a depth of 60 meters.

Figure 1.2. Oil Station

1.1.1.3. Natural Gas

Natural gas is a kind of petroleum derivative energy source, which is mostly gaseous. It is colorless and odorless, but fragranced for safety. Natural gas reserves are generally found in oil deposits or in gas form above these deposits. It can be used without being exposed to any process. It ranks second after oil as fuel. 70-90% of natural gas consists of a hydrocarbon compound called methane gas (CH4). It is easy to store, handle and transport. The widespread use of natural gas began in England in 1790. Natural gas began to be used in the US for the first time in the power generation sector. Natural gas now accounts for 24% of total energy consumption. The world's known natural gas reserves are predicted to have a lifespan of around 70 years.

Figure 1.3. Natural gas station

1.1.1.4. Nuclear Energy

The energy obtained from the fusion and fission reactions of atomic nuclei at high temperatures and high energy is called nuclear energy. Nuclear energy is used in diagnosis and treatment methods for diseases. Nuclear energy is employed in the manufacturing of nutritious foods as well as the purification of dangerous elements found in them. It's also used to clean insects that are damaging to agricultural products, as well as in biochemistry and biology, construction materials, oil tank leak tracking, space technology, and the ship and aviation sectors.

Figure 1.4. Nuclear power plant

Nuclear power plants do not create a greenhouse effect as they do not contaminate carbon dioxide into the air. The fuels used in the nuclear power system can be recycled. Thus, it can be reused as fuel. Obtaining and subsequent development of uranium can also cause serious amounts of radioactive pollution. If the nuclear power plant does not function properly, it can cause massive damage. The Chernobyl disaster that took place in 1986 caused a large-scale disaster. For this reason, it is one of the systems that should be paid the most attention in terms of security measures. The radioactive wastes generated should definitely be prevented from entering nature. Because these radioactive wastes are very damaging not only to nature, but also to the human body.

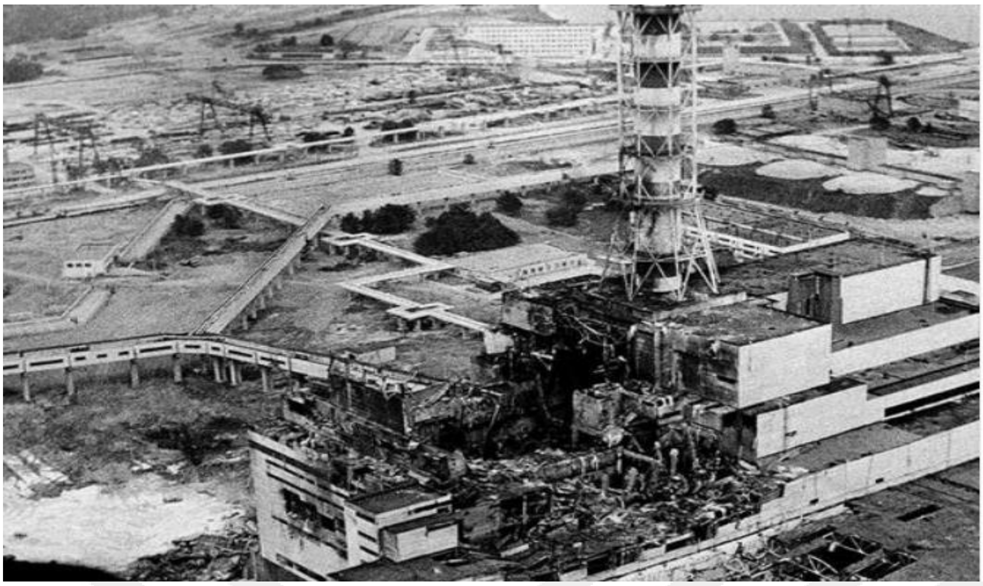

Figure 1.5. An image that emerged as a result of the explosion of the nuclear power plant in Chernobyl

1.1.2. Renewable Energy Sources

Renewable energy sources are energy sources that have a long life cycle and are derived from natural resources. Renewable energy resources include solar energy, hydroelectric energy, hydrogen energy, geothermal energy, sea-wave energy, biomass energy, and wind energy.

1.1.2.1. Solar Energy

Solar energy is created when the hydrogen in the sun mixes and changes into helium, and energy is released throughout the conversion process. The intensity of this radiation is roughly 1370 W/m^2, but due to the earth's atmosphere, the solar energy reaching the Earth fluctuates from 0-1100 W/m^2. This energy does not affect our environment and is a source of energy that all living things require.

In history, when people built their homes , they chose to make use of heat and light, preferring to make use of the sun. In 1725, Belidor invented a solar powered water pump and shed light on the production of a vehicle connected to solar energy. Mohuchok, who invented a steam engine based on solar energy in France in the 1860s, was helped by parabolic mirrors for this invention. People took advantage of heat and light by using too many mirrors in old palaces. After the oil crisis in the 1960s, the search for alternative energy sources was started and led to people getting their needs from different sources. Obtaining solar energy is strategically important as it will not cause any problems between countries.

Solar energy has many advantages and disadvantages:

Advantages;

- Does not harm the environment.
- Sustainable
- Multi-purpose available
- Solar energy is not dependent on outside. It eases the economic situation of the countries.

Disadvantages;

- Solar energy is an inspired energy source. Therefore, it cannot be found 24/7.
- Solar energy has high initial investment costs. It pays off in the long run.
- In order for systems that make use of sunlight to receive sunlight continuously, the environment should be open and not shaded.
- Storage facilities are costly and limited.

Figure 1.6. Solar energy

1.1.2.2. Hydroelectric Energy

Electric energy is generated by converting the potential energy of water flowing from one point to another into kinetic energy. The water is poured down from a great height into a channel or pipelines. This water flows into the turbines, where it is transmitted and turned. Turbines are linked to generators, which transform mechanical energy into electrical energy.

There are six different types of hydroelectric power plants. These;

1. Based on storage structures
2. Based on their height
3. In accordance with their pre-installed abilities
4. In accordance with the conditions of satisfying the national power system's load
5. Based on the typology of the dam body
6. Depending on the location of the power plant's structure

Hydroelectric energy has many advantages and disadvantages:

Advantages;

- Do not harm the environment by not producing greenhouse gases.
- Due to using water, hydroelectric energy does not need to use fuel
- Operational maintenance costs are low.
- Hydroelectric energy is used in irrigation systems.
- Sustainable
- Energy storage and transmission is simple.
- Hydroelectric energy is not foreign dependent

Disadvantages;

- The initial investment cost is very high.
- Installation takes a long time.
- Hydroelectric energy affects the vital activities of aquatic creatures and disrupts the aquatic ecosystem.
- The increase in energy production depends on the amount of precipitation.

Figure 1.7. Hydroelectric power plants

1.1.2.3. Hydrogen Energy

Hydrogen was found in the 1500s, and its potential to burn was discovered in the 1700s. It is the world's and universe's most basic and abundant element. It is a colorless, odorless gas that weighs 14.4 times less than air and is completely non-toxic. Hydrogen is not a natural fuel, they exist in the form of compounds and the most well-known compound is water. Pipelines or tankers can carry the hydrogen produced across long distances. The removal of barriers to hydrogen transportation expands the range of applications. It is very important to use water while generating hydrogen energy. Because there will be no emission of harmful gases, chemicals and greenhouse gases that will pollute the environment.

Hydrogen can be burned in the same way as gasoline and natural gas are. The advantage of oil derivatives over fuels is that they produce fewer emissions. Internal combustion engines for automobiles and hydrogen turbines for military and industrial use have both been developed. Hydrogen is used as energy by generating energy through fuel cells. Fuel cells are materials that work as the opposite of electrolysis. An electric current is obtained by combining hydrogen and oxygen in the air. It is more efficient than burning and is more preferred method. Fuel cells, which are used by NASA in space studies, have also been used in the transport, industrial and service sectors in recent years. Fuel cells can be used in electronic devices such as laptops, mobile phones, as well as suitable power providers for power plants.

Hydrogen energy has many advantages and disadvantages:

Advantages;

- Does not harm the environment.
- Sustainable
- Hydrogen energy has a wide range of uses.
- Hydrogen energy is easy to store and transport.
- Hydrogen energy is more efficient than fossil fuels.

Disadvantages;

- The odorless hydrogen poses a risk in the event of a leak.
- Hydrogen energy is more expensive and costly than other fuels.

1.1.2.4. Geothermal Energy

Geothermal energy is energy obtained from hot water or liquid steam located at certain depths of the Earth's crust, at a temperature higher than 20 degrees, and can contain minerals, various salts and gases. It is usually obtained from the water coming out of cracks and fractures that reach the Earth from within the Earth, or by drilling wells.

The heat inside the earth heats the fluids that are in the rocks or circulating in liquid and gaseous form through various conduction ways. It has a higher concentration of melting minerals, salts, and gases than regular ground and surface waters. Geothermal energy is the most essential alternative energy source to fossil fuels since it is renewable, sustainable, limitless, inexpensive, dependable, ecologically benign, and domestic.

The temperature composition of geothermal energy divides it into three classes;

- Fields with low temperatures of 20°C to 70°C
- Fields with a medium temperature range of 70°C-150°C
- Fields with high temperatures: >150°C

Low and medium temperature fields are used in industrial areas, chemical production and for heating. In addition, medium temperature fields are also used for electricity generation. High-temperature fields can be used in other areas as an integrated besides electricity generation.

The usage areas of geothermal energy are given below:

Table 1.1. Usage areas of geothermal fluids depending on temperature

Temperature(°C)	Usage areas of geothermal fluids depending on temperature
180 °C	Electric power generation, paper industry, cooling by ammonia absorption, high concentration evaporation processes
170 °C	Electricity generation, heavy water and hydrogen sulfide processes, diatomic method material drying processes
160 °C	Conventional power generation, fish and wet lumber drying
150 °C	Aluminum production by Bayer method, conventional power generation
140 °C	Drying of agricultural products quickly, conventional power generation
130 °C	Evaporation in sugar refining, conventional power generation

120 °C	To obtain clean water and salt, sugar production industry
110 °C	Cement drying, evaporation, wool washing and drying
100 °C	Fruit and vegetable, pulp drying processes
90 °C	Volume heating
80 °C	Cooling by lithium bromide method
70 °C	Industrial process water
60 °C	Barn, coop and greenhouse heating
50 °C	Hot water treatments, mushroom cultivation
40 °C	Soil heating
30 °C	Fermentation, distillation, wellness facilities, swimming pools
20 °C	Fish farms

As can be seen in Table 1.1, geothermal energy is used in various areas at different temperatures. It is actively used in areas such as heating, cooling, drying processes, health, especially in electrical energy production.

Geothermal energy has many advantages and disadvantages:

Advantages;

- Geothermal energy is a renewable energy source that is good for the environment.
- Geothermal energy is not reliant on outside sources.
- Efficiency is very high
- The commissioning time of geothermal power plants is short.
- There is a continuity of energy production.
- Investment cost is low.
- Energy produced from geothermal resources is not affected by climate changes.

Disadvantages;

- Preparation and research costs are high.
- Geothermal systems must be close to residential areas.

- Drilling equipment require a wide area to be installed.
- Liquid substances pollution from geothermal sources
- There are harmful chemicals in their structure

Figure 1.8. Geothermal energy

1.1.2.5. Wave Energy

Wave energy is a sustainable energy source that takes advantage of the force provided by waves in the ocean. Although wave energy is the most dependable of the renewable energy sources, it is not a very impressive source of energy. The least used renewable energy source is wave energy. With the help of waves, electric energy is generated by moving the propellers of turbines located in the water.

Wave energy has many advantages and disadvantages:

Advantages;

- Wave energy is less dependent on foreign sources.
- Creates employment.
- Wave energy does not pollute the environment, it is clean and unlimited.
- No toxic gas emissions.

Disadvantages;

- Being close to residential areas
- Insufficient information because of it is a new technology

- Depending on weather conditions
- Affecting the vital activities of sea creatures

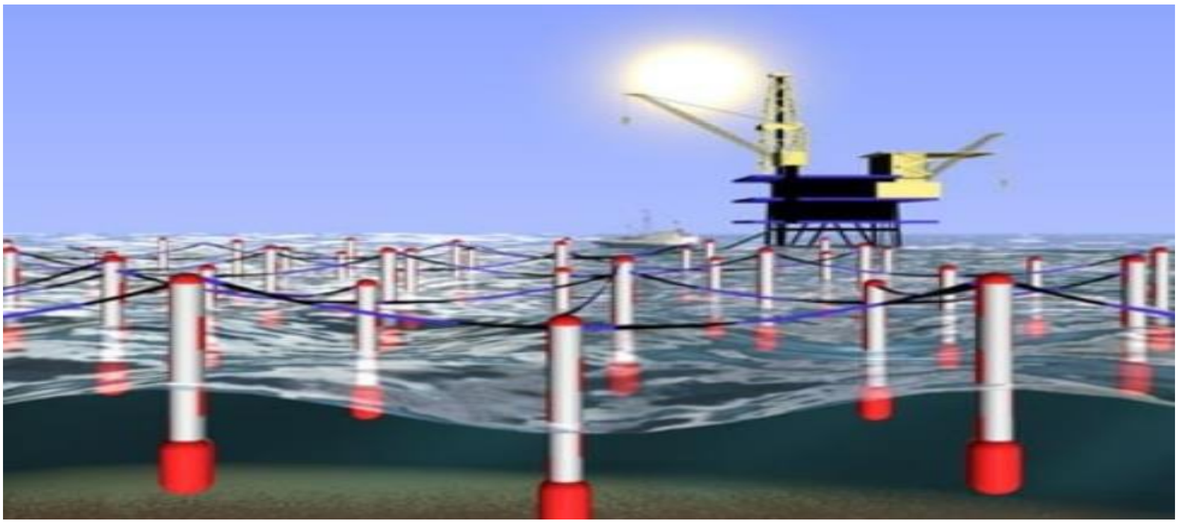

Figure 1.9. Wave energy

1.1.2.6. Biomass Energy

From forest and forest products, all organic substances containing vegetable oil waste, organic waste, agricultural harvest waste are called biomass. Biomass is a source of energy and is used to obtain fuel from biological substances or for other industrial purposes. Solid, liquid, and gas fuels can all be made from biomass. As a result, major goods like biodiesel, bioethanol, and biogas are produced.

Biodiesel is a fuel that is released as a result of the reaction of organic oils derived from oilseed plants such as soy, rapeseed, safflower, sunflower with alcohol such as methanol or ethanol accompanied by a catalyst of base and animal fats.

Biyoetanol is a type of fuel produced from various agricultural products based on cellulose, such as corn, sugar beet. Because it is produced with agricultural products, it is seen as a clean and renewable energy source. The amount of carbon dioxide released as a result of burning this fuel is quite low compared to coal, oil and natural gas.The reason for this is that bioethanol improves the engine performance of vehicles, prevents the engine from freezing, and keeps injectors cleaner.

Biogas is the conversion of organic wastes into carbon dioxide and methane gas with the effect of microbiological flora in an oxygen-free environment. Vegetable wastes or animal fertilizers are used as basic materials for biogas production. It is used as a basic material in the world as the animal fertilizers used are more useful as fermentation during conversion to biogas.

Biomass energy has many advantages and disadvantages:

Advantages;

- Plants produced for biomass energy can be grown in most areas
- Good knowledge of production technologies
- Biomass energy is easy to store.
- Low light intensities are sufficient for biomass energy.
- Temperature between 5-35 °C is sufficient.
- Creates employment.
- Environmentally friendly

Disadvantages;

- Biomass energy can be applied in large residential areas.
- Biomass energy causes strife in agricultural areas.
- Excess water is needed
- Biomass energy is insufficient in terms of efficiency.

Figure 1.10. Biomass energy

1.1.2.7. Wind Energy

The source of the wind is the sun, which is sustainable and natural. Sun rays create temperature, pressure and humidity in various areas due to the shape of the Earth. Forces arising from the different heating and cooling of the earth create air movements. These air masses move from the colder and high pressure area to the warmer and low pressure area, creating the wind. The kinetic energy created by the wind in the continuity of these movements is called wind energy. Wind energy is a renewable energy source that does not harm the environment and the atmosphere, is clean, reliable, has free resources and is among the most preferred.

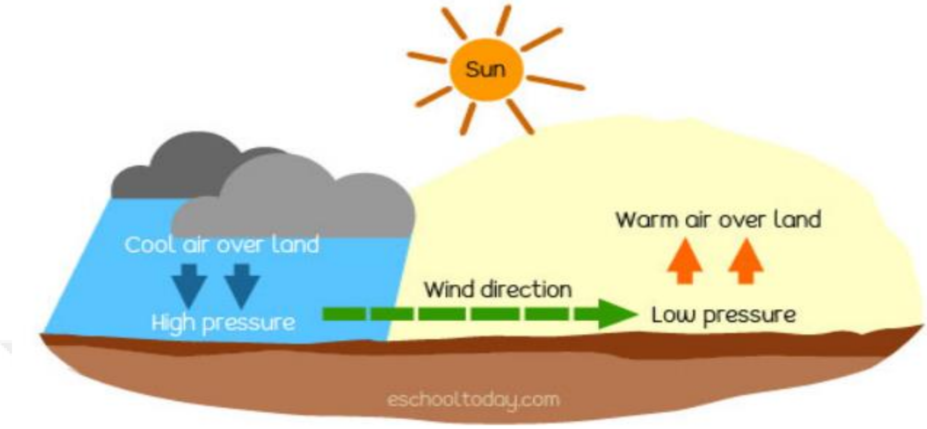

Figure 1.11. An illustration of the formation of the wind

1.1.2.7.1. History of Wind Energy

It is known that the wind energy from BC to the present day, starting in the previous century. People traveled at sea using the wind, sailing ships, used windmills to grind wheat, built irrigation systems to water their crops. Today, wind energy can be converted into usable energy thanks to wind turbines. The wind turbine was first built in Denmark in the 1890s and approximately 25% of the electricity used was produced by wind turbines.

The first turbine produced in 1891 was designed in Denmark by Paul La Cour, with a diameter of 23 meters, a power of 18 kW and 4 blades. Later, in the 1900s, more powerful wind turbines began to be built in Germany and America. Although the energy produced at the beginning was low, the development and production of wind turbines increased in order to prevent the countries consuming fossil fuels and the damage caused to the environment as a result of this consumption.

The first wind power plant in Turkey, Izmir, Alacati town which is 7 km from the village was founded in Germiyan. The power plant was put into operation in February 1998. With a total installed power of 1.5 MW, our power plant produces an annual average of 4 million kWh of electrical energy with 3 wind turbines of 500 kW and meets the electricity of approximately 1,626 residences.

Figure 1.12. Alize-Çeşme wind power plant

1.1.2.7.2. Wind Turbine Components

Wind turbines: it consists of anemometer, blades, brake, controller, gear box, generator, high-speed shaft, low-speed shaft, nacelle, pitch, rotor, tower, wind direction, wind vane, yaw drive, yaw motor components. Thanks to this equipment in the turbine, energy is obtained from the wind.

- **Anemometer:** It measures the speed of the incoming wind and allows it to be transmitted to the control unit.
- **Blades:** The wind that hits the turbine blades moves the blades, causing the blades to rotate. It converts the kinetic energy of the wind into mechanical energy and transmits it to the shaft.
- **Controller:** It turns the machine on and off at certain speeds or speeds.
- **Gearbox:** The gearbox increases the speed of the low speed shaft and connects it to the high high speed shaft. Thus, the number of cycles required for electricity generation is reached. The gearbox is the heaviest and most expensive part in wind turbines.
- **Generator:** Generators convert the mechanical energy generated by the wind turning the blades into electrical energy. Three different generators are used in wind turbines, namely DC generators, synchronous and asynchronous generators. Today, synchronous and asynchronous generators are used mostly for large and medium sized turbines. Asynchronous generators are more preferred in turbines because of their low cost, cheaper and less need for maintenance.
- **High-Speed Shaft:** It activates the generator.

- **Low-Speed Shaft:** It allows the turbine to continue its cycle at low speed.
- **Nacelle:** It is the section that includes gearbox, generator, motor, low and high speed shafts, controller and brake. It provides security by protecting these components from external factors.
- **Pitch:** It prevents the rotor from turning in very low winds and controls the speed of the rotor.
- **Rotor:** The part between the turbine blades and the hub is called the rotor..
- **Tower:** It allows the turbine blades to rotate safely above the ground. In addition, wind speed has an important place in power generation as it increases with altitude. The tube-shaped tower is the most preferred type of tower. The main advantages are low weight and low cost.
- **Wind Direction:** Determines the design of the turbine.
- **Wind Vane:** It measures the direction of the wind and transmits this information to the yaw driver. Thus, the wind turbine is provided to turn towards the wind.
- **Yaw Drive:** Yaw drive ensures that the rotor is always facing the wind according to the changes in the direction of the wind.
- **Yaw Motor:** Yaw motor powers the yaw drive

1.1.2.7.3. Wind Turbine Types

Wind turbines are designed in many different models. Wind turbines are classified according to their axis of rotation, speed, power, number of blades, wind impact, gear characteristics and installation locations.

1.1.2.7.3.1. Wind Turbines According to Rotation Axis

Although there are many different types of wind turbines, they are mostly characterized by their rotating axis. Horizontal Axis Wind Turbines (HAWT), Vertical Axis Wind Turbines (VAWT), and Inclined Axis Wind Turbines (IAWT) are the three types of wind turbines.

- **Horizontal-Axis Wind Turbines (HAWT):** The axis of rotation of the HAWT is parallel to the wind direction, while the wings are perpendicular. Wind turbines with a horizontal axis are placed on shifting land to capture the most wind from the front. The vast majority of commercial turbines have a horizontal axis. The majority of horizontal axis wind turbines in use today are built to take wind from the front. The rotor turns faster in these turbines as the number of rotor blades decreases. Horizontal axis wind turbines have an efficiency of around 45%. The blade tip speed ratio (λ) is calculated by dividing the wind speed by the rotor blade tip speed.

Here; λ = 1-5 Multi-bladed rotor,
λ = 6-8 Three-bladed rotor,
λ = 9-15 Two-bladed rotor,
λ > 15 Single blade rotor is used.

Figure 1.13. Horizontal-Axis wind turbines (HAWT)

- **Vertical-Axis Wind Turbines (VAWT):** In this turbine, turbine shafts are used instead of blades as in horizontal axis turbines. Turbine shafts are vertical and perpendicular to the wind. The generator and gearbox are installed on the ground in vertical axis wind turbines. Since there is no need to move the generator and gearbox above the ground, the tower is not needed, and therefore the installation cost of the turbine is reduced. Since it takes the wind from every angle, there is no need to turn the turbine towards the wind and no yaw system. Among the vertical axis wind turbines, Darrieus and Savonius type wind turbines are the most widely used.

  - **Darrieus Wind Turbines:** The purpose of the darrieus wind turbine is to generate electrical energy using wind energy. Its wings consist of two aerofoil wings placed vertically. The curved structure of the wings allows the formation of traction force on the two wings. As a result of the difference in pulling force between the concave and convex surfaces of the wings, rotational movement occurs.

Figure 1.14. Darrieus wind turbines

- **Savonius Wind Turbines:** Savonius wind turbines, like the darrieus wind turbine, generate electrical energy by utilizing wind energy. It consists of two or three bucket-like aerofoil wings. Irregular air movements on the wing can be seen in the Savonius turbine. Because such movements impair the Savonius turbine's performance, they aren't employed very often. They are suitable for water pumping or other high torque, low rpm applications.
-

Figure 1.15. Savonius wind turbines

- **<u>Inclined-Axis Wind Turbines:</u>** Wind turbines with rotation axes make an angle with the vertical in the wind direction. This type of turbine has a specific angle between the blades and the rotating axis.

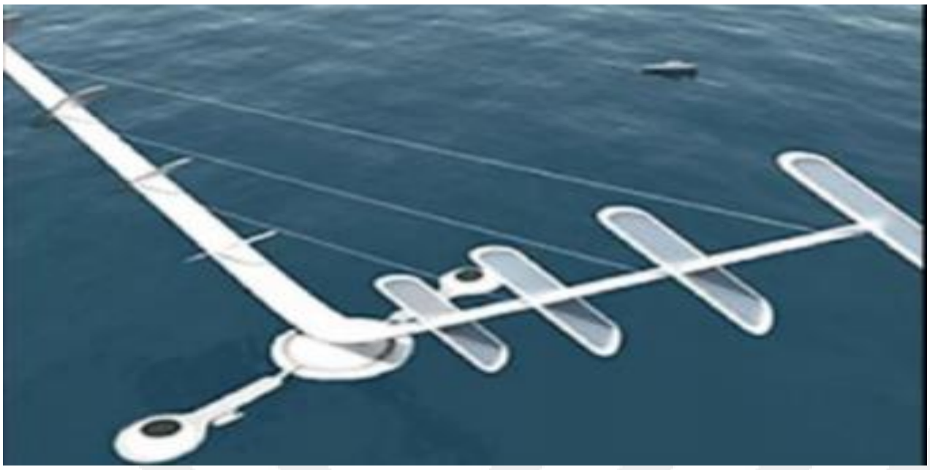

Figure 1.16. Inclined-Axis wind turbines

1.1.2.7.3.2 Wind Turbines According to Blades

According to the number of blades, wind turbines are divided into 4 types: Single blades, double blades, three blades and multi blades.

- **<u>Single Blade Wind Turbines:</u>** To minimize the high rotational speed operating on the propellers, single-bladed wind turbines are used. Due to the aerodynamic imbalance of a single-bladed wind turbine, additional structures should be made to the hub part in order to control the mechanism and provide balance. Since the rotation speed of a single bladed wind turbine is 2-3 times higher than normal, it is a noisy turbine.
-

Figure 1.17. Single blade wind turbines

- **Double Blade Wind Turbines:** Although the two-bladed wind turbine appears to be more cost-effective than the three-bladed wind turbine, they actually cost the same as the three-bladed wind turbine because dynamic effects necessitate more equipment. Double bladed wind turbines have a moment of inertia arising from the rotation of the blades, relative to the horizontal axis of the tower. The extra loading created by this moment can only be eliminated by the swinging core mechanism. Thus, negative moment effects on the rotating propeller are prevented.

Figure 1.18. Double blade wind turbines

- **Three Blade Wind Turbines:** Turbines with three or more blades have a constant moment of inertia. This is why they are the most common turbine models we see today.

Figure 1.19. Three blade wind turbines

- **<u>Multi-Blade Wind Turbines:</u>** Multi-blade wind turbines is the most primitive of wind turbines. In the past it has only been used for pumping water. Multi-blade wind turbines operate at low speed. As the propeller hub goes to the ends, the width of the turbine blades increases.

Figure 1.20. Multi blade wind turbines

1.1.2.7.4. Wind Situation in The World and Turkey

- **<u>General state of wind energy in the world</u>**

Wind energy technology has made great progress since the 1990s, and high-capacity wind power plants have started to be installed. In those years, the installed wind power worldwide was only 2,160 MW, at the end of 1999, the world's installed wind power reached 13,455 MW. This increase continued in the following years, the installed wind power of the world reached 59,091 MW at the end of 2005, 197,956 MW at the end of 2010 and 539,581 MW by 2017.

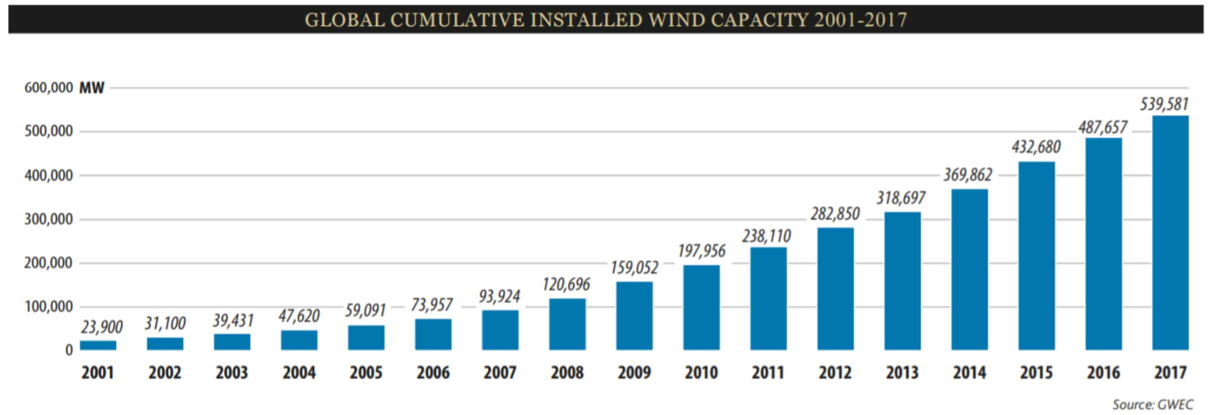

Figure 1.21. Global cumulative installed wind capacity 2001-2017

According to the report of GWEC, the total power of wind power plants in the world has been calculated as 539,581 MW. It has been determined that 188,232 MW of this power is located in China, 89,077 MW in America, 56,132 MW in Germany, 32,848 MW in India and 173,290 MW in other countries.

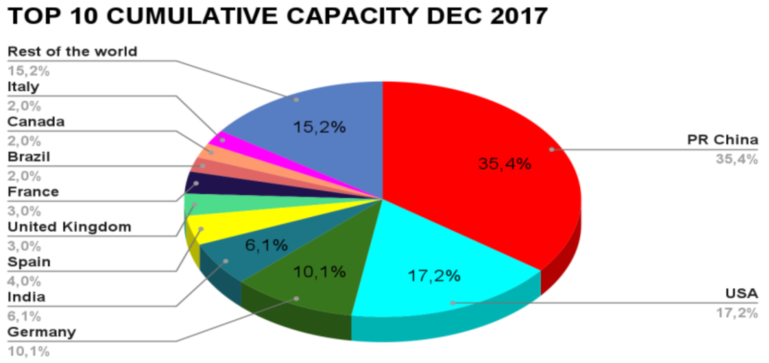

Figure 1.22. The total power of wind power plants in the world

Table 1.2. Countries producing wind energy and the values of the energy they produce in MW

Country	MW
PR China	188,232
USA	89,077
Germany	56,132
India	32,848
Spain	23,170
United Kingdom	18,872
France	13,759
Brazil	12,763
Canada	12,239
Italy	9,479
Rest of the world	83,008
Total Top 10	456,572
World Total	539,581

The vast majority of installed wind farms consist of countries located on the Asian continent, then on the European and American continents, and the rest on other continents. China maintained its lead by increasing installed wind power by 11.55% in 2017. America increased its installed wind power by 8.55%, Germany by 13.55%, and India by 14.45%.,

Looking at the 2016 report published by the International Energy Agency; By using wind energy, a total of 962.896 GWh of electrical energy was produced in the world. In the 2017 report, 1.132.752 GWh of electrical energy was produced, and in the 2018 report, 1.273.409 GWH of electricity was generated.

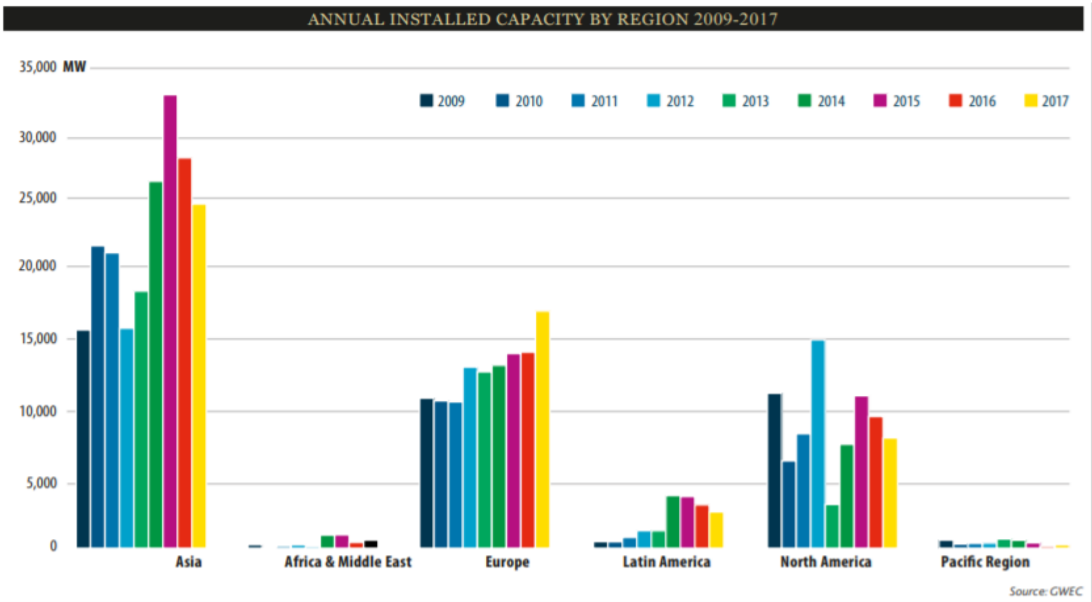

Figure 1.23. Annual installed capacity by region 2009-2017

- <u>**General state of wind energy in the Turkey**</u>

Due to the rapid growth of Turkey's population and technological developments, the demand for energy is constantly increasing. Turkey is among the developing countries. Our country has increased its interest in renewable energy sources in order to reduce its external dependency and meet its energy needs. Unfortunately, the amount of energy can not meet the demand generated by Turkey. Therefore, it allocates most of the energy it needs from foreign countries. That's why, to handle Turkey's wind energy potential in the most appropriate manner and must be used. Turkey wind energy potential atlas is given in Figure 1.26. Among the regions of Turkey, the most favorable region of wind speed is the Aegean region. It is understood that the places where the wind speed is low are the Black Sea Region and the Mediterranean Region.

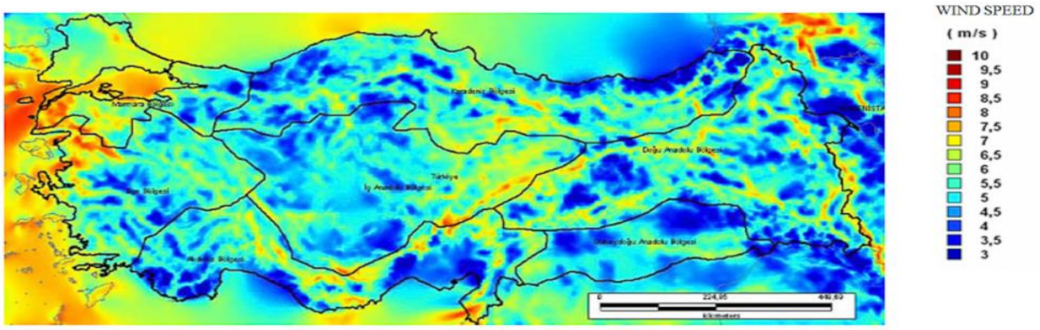

Figure 1.24. Turkey wind energy potential atlas

When we look at the WPP installation power in Turkey between 2006-2019, it is seen that there was an installed power of 51 MW in 2006 and 8,056 MW in 2019. As shown in Figure 1.27, we understand that Turkey is developing wind energy and showing an increasing interest.

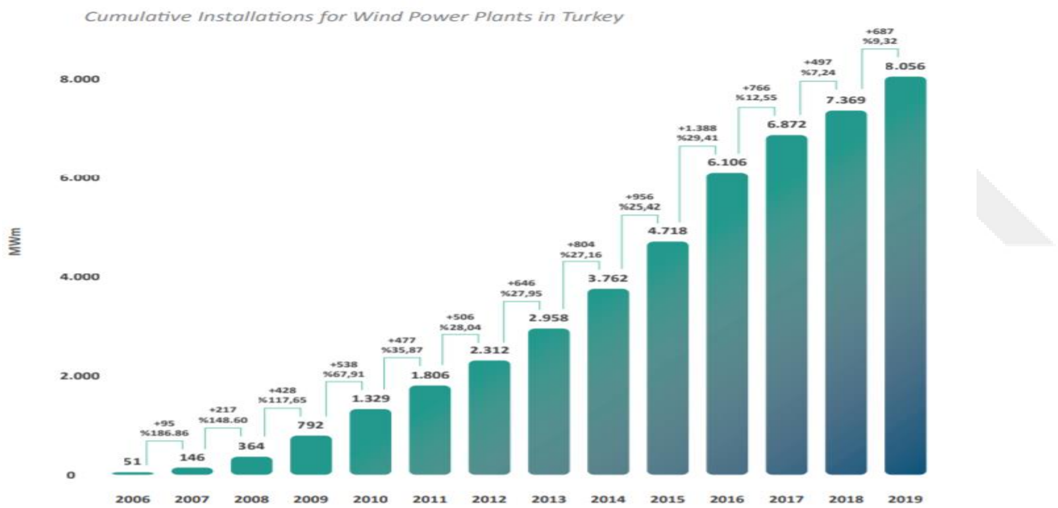

Figure 1.25. Cumulative installations for Wind Power Plant in Turkey

Table 1.3. Turkey's distribution by province of WPPs in operation, the mechanical strength values are shown in terms of percentage and parts are given. While WPP's who were active in Balıkesir in the previous years were in the first place, we see the rapid rise of wind power plants operating in İzmir in 2020.

Table 1.3. Turkey's distribution by province of WPPs in operation and the mechanical strength values

Distribution of WPPs in Operation by City	MWm	%
İzmir	1,549.50	19.23%
Balıkesir	1,163.50	14.44%
Manisa	689.95	8.56%
Çanakkale	594.00	7.37%
Hatay	364.50	4.52%
Afyon	316.45	3.93%
İstanbul	294.10	3.65%
Kayseri	275.10	3.41%
Osmaniye	265.30	3.29%
Others	2,458.55	31.6%

Wind turbines used in wind farms in operation in Turkey; Germany, Denmark, United States, Spain, China, France, belong to different countries such as India and Turkey. Brands such as Nordex, Vestas, Enercon, GE, Siemens, Gamesa, Sinovel, Suzlon, Acciona, Alstom, Senvion, Unison, Northel, Ayetek, Shriram, Milres, Leitwind and Vira are used in these countries. Milres wind turbine is a wind turbine developed by TÜBİTAK within the scope of Milres project (Development of National Wind Energy Systems) and its first 500 kW turbine will be installed on the shore of Terkos Dam in Istanbul and operated by ISKI. In Figure 1.28, Turkey's image in the business of Turbine Breakdown Brand is given.

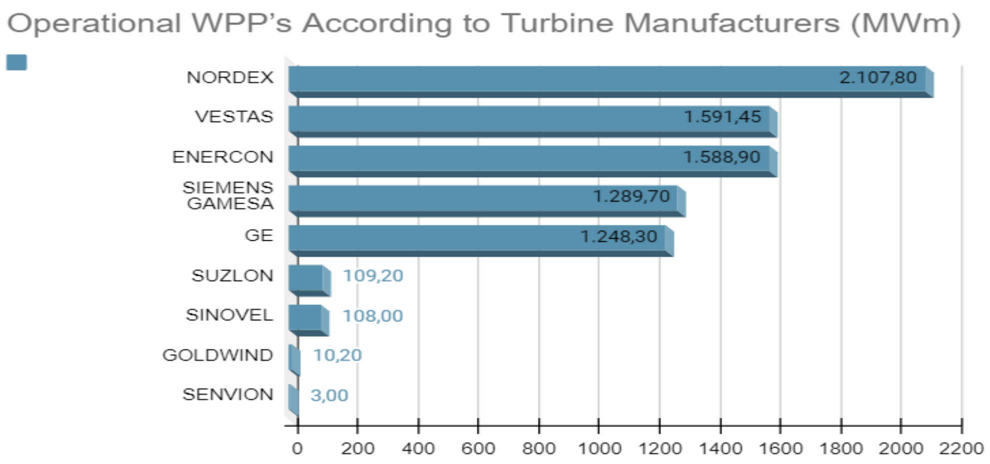

Figure 1.26. Operational WPP's according to turbine manufacturers

1.1.2.7.5. Advantages and Disadvantages of Wind Energy

The advantages of wind energy are as follows;

- Wind energy is a renewable energy source that does not cost fuel during wind power generation. Since it does not use fuel, it does not cause harmful acid rain, harmful gas emissions and greenhouse effect.
- Wind energy is a resource that is not dependent on external sources. It increases the welfare level by reducing the dependence of countries on each other.
- Wind power plants can be used for many years.
- Operating costs are almost nonexistent.
- Wind farms are short to install, simple and easy to maintain.
- Wind energy contributes to regional development by producing jobs in the areas where it is installed.
- Wind farms can be easily dismantled and their land can be easily restored.
- Since the area covered by the turbines is small, agriculture and animal husbandry activities can be continued in the vicinity.

The disadvantages of wind energy are as follows;

- Visual image, noise, and interference in radio and television receivers created by wind turbines adversely affect the inhabitants of that area.

- Dependence on wind speed is one of the biggest obstacles for wind power plants. If the wind is not at a sufficient level, electricity generation is not produced efficiently..
- The high wind turbines endanger the lives of birds. Before the wind farm is established, the migration routes of the birds should be determined and the turbines should be constructed accordingly.
- There is a risk of wind turbines toppling over.

2. LITERATURE REVIEW

Tian Xie et al. (2020) obtained Ni-Fe-P-Nb_2O_5/NF at a lower cost with an electrocatalyst modified with Nb_2O_5. They successfully produced the electrocatalyst Ni-Fe-P decorated with a new Nb_2O_5 on Ni foam by means of nonelectric coating and simple alloy removal. The Ni-Fe-P-Nb_2O_5/NF electrode exhibits excellent electrocatalytic performance against HER requiring only 39.05 mV at a current density of 10 mA cm^2 at 1 M. The electrocatalyst decorated with Ni-Fe-P and Nb_2O_5 shows a high activity. The outstanding electrocatalytic performance and long-term stability of the Ni-Fe-P-Nb_2O_5/NF electrode allow it to be used in general water splitting application.

Meena Nemiwal et al. (2020) summarized the latest developments in heterogeneous catalysis of MOFs for efficient HER and water splitting, and their composites and derivatives. This review discusses strategies to improve stability, efficiency and electrocatalytic properties by giving metal-based classification of MOFs. MOFs have also been used in water splitting for HER and OER. They propose that MOF-based composites and derivatives can be used as electrocatalysts for hydrogen evolution and water splitting.

Shuangshuang Ren et al. (2020) developed a MOF-on-MOF strategy to obtain trimetal-based nitrogen-doped carbon nanotube arrays loaded into nickel foams (referred to as FeNiCo@NC / NF). Research has found that trimetallic FeNiCo nanoparticles can provide better metal active areas, N-doped carbon nanotube arrays linked together can offer more efficient electron transport channels, and the conductive Ni foam substrate can reduce the internal impedance of the material. According to the researchers' studies, they suggest that an excellent material has been produced with potential application in electrode materials for hydrogen/oxygen evolution reactions and water splitting to replace noble metal-based electrocatalysts.

Haishun Jiang et al. (2020) MoS_2/NiS hierarchical nanostructures (HHs) were generated on Ni foam with a straightforward one-step hydrothermal reaction employing Ni foam as the raw material. On the surface, there are many active species and low natural resistance due to the porous nature of Ni foam and the heterogeneous structure of MoS_2/NiS. It is a superb electrocatalyst with an extreme potential of 84.1 mV and a Tafel slope of just 76.9 mV dec^{-1}

when used at 10 mA cm^{-2}. It delivers a cost-effective catalytic hydrogen producing material with great performance and stability, according to the study.

Hua Zhang et al. (2020) discovered in their study that the Ni-Fe-Sn60 electrode had the best electrocatalytic characteristics. In 1 M KOH solution, the electrode generated potential 43 and 120 mV current densities of 10 and 100 mA cm^{-2}, respectively, and a modest Tafel slope of 70 mV dec^{-1}. The electrode has a lot of promise for large-scale applications because of its outstanding electrocatalytic performance, simple synthesis technique, and usability.

Qiaoqiao Zhang and Jingqi Guan (2020) focused on a variety of SACs (monatomic catalysts) containing single or double metal regions, including Mn, Fe, Co, Ni, Mo, Pd, Rh, Ir, and Pt for HER and OER. They documented synthesis methods and characterization techniques of SACs. According to the research, SACs improve their catalytic performance, strong metal support interaction is suitable for creating active and stable catalytic sites. Isolated metal atoms can be added to increase the density of the active areas. TEM, STM and XAS can be used to monitor the dynamic chemical composition and structure of SACs. In order to gain an in-depth understanding of the catalytic mechanisms of SACs for HER and OER, in situ/operative characterization techniques should be used. They say that the combination of electron microscopy and X-ray spectroscopic characterizations can provide important information that will contribute to the rational production of efficient and robust SACs during catalysis.

Using a hydrothermal method, A.A. Yadav et al. (2020) effectively produced highly porous 3D nanoflower-like $CoMoS_4$/NF electrodes. In a strong alkaline environment at low extreme potentials, $CoMoS_4$/NF is an electrocatalyst with many active sites, excellent stability, and good performance for HER and OER processes. At a cell voltage of 1.51 V, an electrolyzer cell using nanoflower-like $CoMoS_4$ for both the anode and cathode produced a current density of 10 mA/cm^2. They came to the conclusion that the $CoMoS_4$/NF catalyst is a useful material for water splitting as a consequence of their research.

Yadav et al. (2020) Sponge ball-like CuO and CuO/rGO photocatalysts were successfully synthesized by a simple hydrothermal method. CuO and CuO/rGO photocatalysts were analyzed using various structural, morphological and optical characterization techniques. It was revealed that the CuO/rGO composite showed superior photocatalytic hydrogen production activity compared to CuO. They observed that the CuO/rGO composite is 3 times more efficient than CuO for hydrogen production.

Kim Hoong Ng et al. (2020) claim that solar powered photocatalytic water splitting is a practically impossible way of using both thermodynamic and solar energy to intentionally generate H_2. They say photocatalytic water splitting, which has been widely studied for H_2 production, does not promise to be used commercially with its low STH efficiency (<10%) and high cost of hydrogen (> 2-4 $ / kg). Although the problems have been overcome, it is impossible to outperform the thermodynamic hurdle of 18% STH as it often needs to be greater than 2.0 eV for significant water splitting. Photon energy losses are inevitable during mid-medium transfer in photocatalytic water splitting, and therefore sacrifice yields the best STH of only 3.32% even in the presence of reagent.

H.Chen et al. (2020) used carbonization and oxidation to make bimetallic carbon nanotube electrocatalysts from Hofmann-type metal-organic frameworks (FeNi@OCNC). FeNi@OCNC activity remained stable for 12 hours, demonstrating that the OER outperforms both single metal and trimetallic electrocatalysts. The findings show that forward-looking materials for the oxygen evolution reaction, such as FeNi@OCNC, may exist.

Guangfu Qian et al. (2020) were prepared by a combination of bimetallic telluride ($CoNiTe_2$/NF) nanosheets, hydrothermal and calcination method. Using the combination of bimetallic telluride and 3D structure, it was determined that it needs 181,230 and 270 mV extreme potential and low Tafel slope (44 mV dec^{-1}) by showing significant OER activity. It also showed good stability after keeping the current density at 100, 500 and 1000 mA cm^{-2} for 24 hours, respectively. Based on their work, the researchers aimed at producing bimetallic telluride and improving OER performance and producing high purity H_2 on a large scale.

Leiming Tao et al. (2020) successfully synthesized ACo2O4 phases (A = Mn, Fe, Co, Ni, Cu or Zn), aiming to examine the effects of cation substitution on OER in spinel cobaltites derived from mixed metal organic frameworks. Among them, $FeCo_2O_4$ spinel oxide showed excellent OER catalytic activities with a current density of 10 mA cm^{-2} at 164 mV extreme potential in an alkaline environment, and they observed that the spinel crystal field electrode materials are suitable for OER performance.

F.Safari and I.Dincer (2020) have done a study of the Iron-chlorine (Fe-Cl) cycle, one of the thermochemical cycles of the chlorine family in which ferric chloride is consumed for hydrogen production from water. They modeled Fe-Cl using Aspen Plus and examined the performance. The results showed that while the hydrolysis reaction resulted in higher magnetite and lower hydrogen production and higher steam/$FeCI_2$ ratio at lower temperatures, the effect of pressure was not significant.

Hybrid water electrolysis, according to Lijie Du et al. (2020), is a safer, more energy efficient, and more lucrative approach to manufacture hydrogen for OER. They provided some recommendations, stating that hybrid water electrolysis is still in its early stages of development and that further research is needed;

- The product should be examined for reaction selection, taking into account several parameters such as separation and purification, membrane degradation, and so on.
- The OER can be fully repressed if the activation potential falls below 1.23 V.
- Changing the anode reaction requires changing the substrates that will be spread over the cathode area.
- As a result, they believe that hybrid water electrolysis will eventually come into practical application.

Shaoting Zhao et al. (2020) developed $NiCo_2O_4$/CF-P as an electrode for OER, under the cooperation of small size morphological effect and heteroatomic doping activity. This material developed showed a low extreme potential of 191 mV at 10 mA cm^{-2} in alkaline solution and a ten-year Tafel curve of 83 mV. The $NiCo_2O_4$/CF-P electrode with improved HER activities superior to $NiCo_2O_4$/CF during a 30-hour test It exhibited excellent long-term electrochemical stability. They say it is an advantageous method to increase the active areas exposed to better place electrocatalysis in water splitting.

Xiaocong Gu et al. (2020) demonstrate in this work that fluorination of a Prussian blue analog hollow nanobox with a ZIF-67 Frame pattern is highly efficient for OER. For OER, the ZIF-67@CoFe-PBA-F-250 catalyst performed better compared to the IrO_2 catalyst. Specifically, in a chronoamperometry test 34 mV dec^{-1} provided 243 mV extreme potential at 10 mA cm^{-2} current density with a small Tafel slope and remarkable stability for 12 hours. Its catalytic performance extends the application of MOF / PBA derivatives in electro-catalysis for water splitting reaction in terms of rich active sites, large surface area and efficient charge transfer capability.

C.Schnuelle et al. (2020) found that key performance indicators (KPIs) such as hydrogen generation efficiency, electricity utilization rate, output and net production costs depend heavily on the shape of transient power input signals and the ability of electrolysers to deal with them. Economically, AEL (alkaline electrolysis) technology is preferred for direct renewable electricity powered electrolyzer operation. While PEMEL (polymer electrolyte membrane electrolysis) technology generally has higher electricity usage rates than AEL, AEL achieves large hydrogen generation amounts due to its higher efficiency.

Shasha Zhu et al. (2019) have sequentially synthesized the CoO/NF electrode using cobalt chloride hexahydrate, urea and NF substrate with hydrothermal reaction and calcination process. The results of the electrochemical tests show that CoO/NF has excellent catalytic activity with 307 mV extreme potential for OER at 10 mA cm^2 current density, and CoO/NF catalyst provides 10 mA cm^2 current density for HER at 224 mV extreme potential. CoO/NF has outstanding stability. CoO/NF catalyst showed improved performance due to reduced load transfer resistance and active zone. They have shown CoO/NF to be a promising material to replace noble metal-based catalysts.

Shuxian Zhuang et al. (2019) in their work, dense $NiMoO_4$ micropillar arrays (MPAs) were grown in situ on nickel foam (NF) by the easy hydrothermal method, then converted to $NiMoO_4$/NF, phosphating and electrodeposition to $NiMoO_4$-P/NF and NiFe/$NiMoO_4$/NF. These transformed materials show low extreme potential for HER and OER, small Tafel slope and high stability. The researchers' work has promised the future to create HER and OER catalysts for the manufacture of low cost materials with water splitting performance.

Linzheng Ma et al. (2019) effectively structured a 3D bifunctional electrode for water splitting made of vanadium-doped Ni_3S_2 nanosheets built on carbon fiber fabric (V-Ni_3S_2/CC). The Ni_3S_2 catalyst contributes to improved intrinsic activity and quicker catalysis reaction kinetics. Vanadium additions have a good effect on the catalysis process. They discovered that the V-Ni_3S_2/CC electrode could be employed for effective water splitting applications and that low extreme potentials of 180 mV for OER and 81 mV for HER at 10 mA cm^{-2} exhibited high catalytic activity as a consequence of the research. V-Ni_3S_2/strong CC's catalytic performance for water splitting should be attributed to:

- Between the catalyst and the electrolyte, the sheet-like shape provides a large catalytic area.
- The array architecture of edge-terminated V-Ni_3S_2 nanosheets provides conveniently accessible catalytic sites as well as benefits for charge exchange, electrolyte penetration, and intermediate transforms.
- Vanadium dopants improve the intrinsic activity of the Ni3S2 catalyst while also speeding up the catalysis reaction kinetics.

Transition metal oxide Fe_2O_3 nanocatalysts on N-doped carbon nanomaterials show good electrocatalytic performance for hydrogen generation process in an alkaline environment, according to Jibo Jiang et al. (2019). The Tafel slope is 76.6 mV dec^{-1}, and with a 245 mV extreme potential, Fe_2O_3-NCs-800 has good electrochemical kinetics and low overpotential, according to the data analysis and calculations. The Fe_2O_3-NCs-800 electrocatalytic material's hydrogen evolution persisted for 48 hours below 350 mV extreme potential, indicating that the material's electrochemical stability is outstanding. They have recommended Fe2O3-NCs-800's usefulness as an essential promising material for industrial hydrogen evolution because the synthesis procedure is straightforward and raw components are inexpensive and easy to obtain.

Linwei Jiang et al. (2019) used a one step hydrothermal process to create the CoS_x-Ni_3S_2 nano-sheet array electrode. By emphasizing electrode superhydrophilicity and supererophobicity, nanoarray architectures allow easy access of electrolytes to the active regions of the catalyst and quick gas diffusion. In an alkaline environment, the proposed electrode demonstrated remarkable dual function activities, requiring just 1.63 V to support 100 mA cm^{-2} current density and demonstrating excellent durability for 20 hours at 20 mA cm^{-2}. The researchers were able to model and witness the process of solar and wind energy generating electricity in laboratory circumstances to power water splitting for hydrogen synthesis using the CoS_x-Ni_3S_2 nanosheets array electrode. The researchers propose that CoS_x-Ni_3S_2 be employed for future large-scale water splitting applications based on their findings.

B. Lai et al. (2019) report their research by presenting a scalable synthesis method from abundant materials, synthesis of low-layer MoS_2 nanoparticles, NiO nanoparticles (NPs) and multi-walled carbon nanotubes (MWCNTs). Every performance of several layers of intact MoS_2 nanoflakes, MoS_2/NiO NPs and MoS_2/NiONPs/MWCNT nanocomposite electrocatalysts were investigated in acidic and alkaline environments. MoS_2 nanosheets synthesized with NiO NPs showed excellent performance for OER with ~60 mA/cm^2 anodic current and 78 mV dec^{-1} Tafel slope in alkaline environment. Performance parameters such as initial potential, current density, Tafel slope in alkaline medium and MoS_2 nanosheets with surface function in alkali medium are higher compared to acidic electrolyte.

The work of A.Landman et al. (2019) reveals solar water separation in separate oxygen and hydrogen cells. Over standard PEC cell topologies, separating hydrogen and oxygen production into two cells electrically coupled by nickel hydroxide/oxyhydroxide auxiliary electrodes offers substantial advantages. The PEC-PV configuration has been developed to maximize system efficiency and to reduce the swap frequency and system cost of auxiliary electrodes by optimizing the cycle process and cell arrangement of the auxiliary electrodes. Ten steady water splitting cycles (each cycle period was 8.3 hours) with an average current of 55.2 mA and a solar-hydrogen activity of 0.68% were used to evaluate system performance. Finally, paralleling a 25 U load to the PEC system for simultaneous hydrogen and electricity generation resulted in a 2.5-fold gain in efficiency and an overall efficiency of 1.7%.

A.Krishnan et al. (2019) were successfully prepared from TiO_2/PANI nanocomposite, titanium metal chips and aniline by in situ polymerization reaction. By evaluating the crystallinity of the composite by X-ray diffraction analysis, the long-term activity of the composite for the photocatalytic water splitting reaction confirmed the industrial importance of the catalyst composite.

D.Zhang et al. (2019) employed a one-step solvothermal approach to make amorphous MoS_x nanorods grown on Ni_3S_2 and direct Ni foam (Ni_3S_2-MoS_x/NF) as a high-efficiency electrocatalyst for general water splitting. At 1.0 M KOH, the Ni_3S_2-MoS_x/NF composite has exceptionally low extreme potentials of 65 and 312 mV, allowing it to approach 10 mA cm^{-2} and 50 mA cm^{-2} for HER and OER, respectively. It also has a low Tafel slope (81 mV dec^{-1} for HER and 103 mV dec^{-1} for OER), a high variation current density (1.51 mA cm^{-2} for HER and

0.26 mA cm^{-2} for OER), and outstanding long-term cycle stability. They claim that the MoS_x/NF composite has a high efficiency and enough stability for widespread water splitting. The researchers offered a fresh viewpoint to the task, focusing on non-precious metal elements that are extremely efficient in the energy market.

Z.Wang et al. (2019) created a core-shell structured 3-D Ni_3S_2@$Co(OH)_2$ nanowires as a bifunctional catalyst for OER and HER after thinning directly onto nickel (Ni) foam. The Ni_3S_2 nanowires are equally wrapped in an incredibly thin layer of α-Co(OH) 2 nanosheets. They discovered that the 3-D Ni_3S_2@$Co(OH)_2$ nanowires they created had a positive impact on electrocatalytic processes and performance. Because of the low starting potential, the Ni_3S_2@$Co(OH)_2$ electrocatalyst displayed superior HER and OER electrocatalytic performance in terms of reduced excess potential and increased durability. Using Ni_3S_2@$Co(OH)_2$ as the bi-functional catalyst in the water electrolyser, high HER and OER performance indicated that HER and OER were electrocatalytically stable during water splitting for 100 hours. They indicate that Ni_3S_2@$Co(OH)_2$ can be employed as a potential and alternative bifunctional electrocatalyst material for alkaline water electrolyzers because of its strong HER/OER activity and stability in the KOH electrolyte.

In order to water splitting, Li An et al. (2018) employed preservation and subsequent controlled sulfurization to make N-$NiMoO_4$/NiS_2 with numerous epitaxial heterogeneous interfaces. They claim that in alkaline circumstances, the N-$NiMoO_4$/NiS_2 electrocatalyst has a high HER activity and good OER performance. By facilitating the release of H_2 and O_2, a 2D nano-leaf supererophobic, binder-free 3D open electrode on CFC (carbon fiber cloth) improves the HER/OER property and stability. This water-alkaline electrolyser on the CFC uses N-$NiMoO_4$/NiS_2 as both the cathode and anode electrodes and has a modest cell voltage of 1.60 V at 10 mA cm^{-2} for steady overall water splitting. As a result, they claim that the N-$NiMoO_4$/NiS_2 electrocatalyst illuminates the future of sustainable energy generation.

Floating photovoltaic systems with integrated hydrogen production units, as used in Turkey's Aegean Mumcular investigated with electricity demand data received from the Dam by M. Temiz and N. Javani (2018). They have used PvSyst and HOMER Pro software programs. The hydrogen produced was used to meet electricity needs when solar energy was not available in the fuel cell's generator, the land was saved, the damage to the environment was reduced. The system is commercially available. The fuel cell generator that produces and stores hydrogen has proven to be a good alternative and greatly reduces unmet electricity in the floating PV system.

H. Ishaq et al. (2018) investigated a solar-wind hybrid system for hydrogen generation using the Cu-Cl cycle. The wind turbine generates power, while the solar heliostat field provides the heat energy required for increased hydrogen production rates. On the basis of energy and exergy efficiency, a full performance assessment of the system is conducted. The solar helicopter in the planned system has an area of 11 m × 11 m and receives 0.85 kW/m^2 of direct normal irradiation. The total power output of the wind turbines is 11.98 MW. As a result, a 455.1 kg/hour hydrogen production rate is produced and stored at 25 C° and 750 bar pressure.

Lishan Peng et al. (2018) have rationally designed bifunctional electrocatalysts for general water splitting of monometallic $NiO-Ni_3S_2$ heteronanosheets supported on Ni foam. Due to the unique electronic property of the abundant interface and the 3D interconnected integration structure, $NiO-Ni_3S_2$ heteronanosheets exhibited high electrocatalytic activity for HER and OER. They observed that $NiO-Ni_3S_2$ performed better than the RuO_2-Pt/C pair for water splitting. $NiO-Ni_3S_2$ accelerates water splitting, its excellent activity and satisfactory durability make it a promising bifunctional electrocatalyst for water splitting in a strong alkaline environment.

F.Safari and I.Dincer (2018) proposed and analyzed an integrated wind power system for hydrogen and methane production for better energy performance and more methane production, and achieved optimal working standards. There are 44% total energy and 45% exergy yields, respectively. However, independent of the aerodynamic features of the wind blades, the study's findings reveal that increasing windless speed increases the rate of exergy destruction and lowers exergy efficiency while increasing methane generation. When 60.2 kW of wind-based power is used at a production rate of 0.78 kg/h CH_4 in the base scenario, 2.27 kg/h of CO_2 is caught. To discover the best point and trade-off between exergy efficiency and methane generation, a multi-purpose optimization research was conducted.

T. Manovah David et al. (2018) aimed to obtain H_2 by water splitting process using titania (TiO_2) nanotubes (NTs) prepared by fast splitting anodization. To investigate the efficiency of water splitting, they tried anatase TiO_2 sensitized with Pt, Pd and Ni nanoparticles (NPs). Morphological examination using FESEM and TEM clearly shows that TiO_2 NTs are obtained in bundles with NPs as spherical deposits on it. SAED and XRD models confirmed the anatase structure of TiO_2 NTs and FCC (face centred cubic) structure metal NPs. Reducing the intensity of radiation is proof that Pt/TiO_2NTs perform better.

Chengrong Wu et al. (2017) successfully synthesized 3D curved nano-layers of Mo-doped Ni_3S_2 grown on nickel foam in a one-step hydrothermal process. As a result of detailed investigation of the HER and OER in the alkaline environment of the 3D catalyst, they found that both OER and HER have lower extreme potential, high current densities and small Tafel slopes. The researchers' work turns out to be a low cost and efficient bifunctional catalyst electrode in water splitting to produce both O_2 and H_2 in alkaline solution.

Yuan Rao et al. (2017) have made a proposal for in situ cultivation of NCDs on Ni foam (NCDs/Ni_3S_2/NF) by hydrothermal treatment of Ni foam in water solution of thiourea and NCDs. It has been observed that the obtained NCDs/Ni_3S_2/NF composites can be used as general direct self-supporting electrodes providing a current density of 10 mA cm^{-2} at 1.50 V with excellent durability in 1.0 M KOH solution for water splitting. Coral-like NCDs/Ni_3S_2/NF composites have superior catalytic activity and durability, saying they can be used directly as both anode and cathode for water splitting.

Through a partial cation exchange reaction between NF supported Ni_3S_2 nanosheet arrays and cobalt (II) ions, Yuanyuan Wu et al. (2017) have documented the production of such a catalyst incorporating ultra-fine Ni_xCo_{3}-$_xS_4$ decorated Ni_3S_2 nanosheet arrays supported on nickel foam (NF). For both HER and OER, the material developed proved to be a very efficient and super stable electrocatalyst. By performing a partial cation exchange reaction between NF supported Ni_3S_2 nanosheet arrays and Co (II) ions, Ni_xCo_{3}-$_x$S4 ornamented nickel foam (NF) supported Ni_3S_2 nanosheet arrays were effectively manufactured. A high-performance electrolyser for the general water splitting process has also been shown, with Ni_xCo3-$_xS_4$/$N_{i3}S_2$/NF as a bifunctional electrocatalyst at both the anode and cathode. According to them, the findings reported here might be beneficial. The findings might open the way for the creation of extremely effective water splitting electrochemical devices, according to the researchers.

D.Martinez and R.Zamora (2017) discussed the application of a MATLAB/ Simulink/Simscape power system of an alkaline electrolyser directly coupled to a photovoltaic module. They added a variable input to measure the response of the models to temperature and a variable resistor for the PV module. They observed that the voltage variation for certain temperatures did not affect the PV module acting as a current source proportional to module heating. The amount of electrical energy entering the system changes seasonally. There was more electricity input in the summer than in the winter. The efficiency of the electrolyzer is higher in the summer months.

Tahereh Jafari et al. (2016) discussed chemical reactions, physicochemical conditions, and types of photocatalysts such as metal oxides, sulfides, nitrides, nanocomposites, and doped materials, and then various aspects in computational modeling of photoactive materials. They consider the development of a visible light-absorbing, small particle size flaw-calibrated material that is resistant to photocatalytic corrosion is the key to effectively completing the hydrogen cycle from sunlight. They say the current view of efficient water splitting is based on an innovative photocatalytic material design. Heterojunctures involving carbon-based material are believed to be one of the future viable ways to design efficient photocatalysts.

Junjie Li et al. (2015) carried out one-step synthesis of Ni_3S_2 nanowires at low temperature as an efficient electrocatalyst for the hydrogen evolution reaction. For HER and OER, the Ni_3S_2-MoS_x/NF composite has very low extreme potentials. It also has a low Tafel slope, a high exchange current density, and a long-term cycle stability that is outstanding. They claim that the MoS_x/NF composite has a high efficiency and enough stability for widespread water splitting. The researchers introduced a fresh viewpoint to the task, focusing on non-precious metal elements that are extremely efficient in the energy sector.

C. Ouyang et al. (2015) used a simple hydrothermal technique with HCl pre-treatment to effectively manufacture the hierarchically porous Ni_3S_2 nanorod array foam. They discovered and reported that hierarchically porous Ni_3S_2 nanorod arrays on AT-Ni foam had good electrocatalytic activity against HER and OER, with low over-potentials of 200 mV and 217 mV, respectively, and current densities of 10 mA cm^{-2}. The nanorod array structure provided quick routes for mass transport and electron transfer, the porous structure gives wide surface area that may expose more active sites for electrocatalysis of HER and OER, and its stability was considerably enhanced. As a result, Ni_3S_2/AT-Ni foam is a viable option. As a result, Ni_3S_2/AT-Ni foam has the potential to be a low-cost, high-efficiency electrocatalyst for both HER and OER.

Liang-Liang Feng et al. (2015) developed a synthetic approach for growing Ni_3S_2 nanosheet arrays on nickel foam with a high index orientation. The use of Ni_3S_2 as a very efficient electrocatalyst for HER and OER has been established. They showed that the excellent catalytic activity of Ni_3S_2/NF is due to the synergistic catalytic effects produced by their nanosheets and high index surfaces. Density functional theory calculations were made to understand the catalytic activities of high index and low index Ni_3S_2. By comparing the surface energies, it was seen that the most stable surface was high indexed. As a result; High index surfaced Ni_3S_2 nanosheet arrays were found to catalyze both HER and OER efficiently. In addition, the durability and low cost of Ni_3S_2/NF showed that it should be used instead of metal-based catalysts.

Manabe et al. (2013) they have made basic research on AWE (Alkaline water electrolysis) by detecting technical problems under the zero gap system in the new cell technology. In their research, they observed that the zero gap system operates at a lower cell voltage without causing any problems compared to a conventional finite space cell. Cell design is important for the performance and longevity of the electrolyser and the cell. The oxygen overvoltage of the anode must be kept in balance. The separator is extremely important for the long life, performance and lowering of the system. Zero backlash system can reduce cell voltage in AWE.

Chi-Hung Liao et al. (2012) present a thorough overview of photocatalytic water splitting for hydrogen production. Various research have revealed that sacrificial active components must be continually introduced to achieve long-term hydrogen generation. Improved hydrogen generation was also proven by the creation of novel photocatalytic reactor systems to enable independent H2 and O2 evolution, such as the H-type reactor and the new Z-scheme. They discovered that a variety of synthesis strategies, such as loading metal or metal oxide particles on the photocatalyst and fabricating dye-sensitive composite photocatalysts, may be employed to increase photocatalytic water splitting performance. In addition, for photocatalytic water splitting, a large variety of non-oxide semiconductor materials have made significant development. However, the materials' stability remains a key issue for their use.

B.Olateju and A.Kumar (2011) aim to develop a detailed data-intensive technoeconomic model for the assessment of hydrogen production from wind energy through the electrolysis of water. It is based on the expansion of a wind farm where electricity is produced with hydrogen production. Considering the total cost of hydrogen, the most suitable size for the plant is the largest electrolyzer considered, with 1440 kW (300 Nm^3/hour). They think that the commercialization of the oxygen produced by the electrolyser can also increase the competitiveness of the production price.

M.S. Genç et al (2011) presented the Review study about hydrogen production via wind energy in Niğde, Kırşehir, Devel, Sinop and Pınarbaşı. They have reviewed studies related to the study of hydrogen production costs. Hydrogen production and production cost differences have been compared for different scenarios, different wind turbines and different core heights. As a result of the comparisons, Pınarbaşı and Sinop have a considerable wind potential, therefore hydrogen production can be realized by using both wind energy and wind-electrolyzer energy system. Wind energy conversion and wind-electrolyzer energy systems should be encouraged in Pınarbaşı and Sinop.

Using $Sn_xFe_yO_z$ powders generated from sol-gel, R.Bhosale et al. (2011) explain the creation of H_2 from a thermochemical water splitting process. They were able to effectively produce $Sn_xFe_yO_z$ particles using the sol-gel process, which entails making a sol containing Sn and Fe, gelation with PO (propylene oxide), fast heating, and quenching in an air/N_2 atmosphere. The reacted $Sn_xFe_yO_z$ powders demonstrated that both the air specified phase composition and the mixed phase materials resulted in the same phase composition including $Sn_{0.4}Fe_{2.6}O_4$ and SnO_2, according to X-ray diffraction analysis. The thermochemical cycle, which included reacting air, resulted in a considerable decrease in the stipulated phase composition, as well as the SSA (specific surface area) and porosity of the mixed phase materials. Grain testing proved it. Grain growth was seen during the SEM study, which validated it.

B.W. Jensen and D.R. MacFarlane (2010) research have led to the improved stability of polymers and the development of conductive polymers, creating a new field for their use as electro-catalysts. They also thought it would lead to applications in new fields such as hydrogen oxidation. They suggest that intrinsically conductive polymers such as PEDOT (3,4-

ethylenedioxythiophene) should make a joint effort from scientists and research for electrocatalysts.

G.Peharz et al. (2006) presented an integrated system combining solar cells with a polymer electrolyte membrane electrolyser. In Freiburg, Germany, an efficiency of 18% has been determined for hydrogen production from the sun in outdoor conditions. It can be done by varying the band gap energies for the sub-cell materials in the sequential cell. In this case, solar hydrogen efficiencies> 20% can be achieved. They emphasize that more research needs to be done on replacing titanium plates with cheaper polymer materials, and it is necessary to explore ways to manufacture large area polymer electrolyte membranes and high-quality electrodes at low cost.

Meng Ni et al. (2005) made investigations aiming to review the current development of technologies applied in TiO_2 photocatalytic hydrogen production. As a consequence of the research, applications to boost TiO2's photocatalytic activity have been developed, which have had a favorable impact on hydrogen generation. Combined with the dye sensitive TiO_2 redox mediator loaded by the noble metal, sustainable hydrogen production can be achieved under sunlight. Modeling work is necessary for a better understanding of the hydrogen production mechanism as well as for designing an efficient photoreactor. They anticipate that low-cost, environmentally friendly photocatalytic water splitting for hydrogen production will play an important role in hydrogen production and will contribute a lot to the future hydrogen economy.

S.B. Han et al. (2005) investigated the water splitting reaction utilizing a thermochemical cycle and ferrites to produce H_2. The ferrites were reduced by heat energy during the thermochemical cycle, and they divided the water to form hydrogen with the decreased ferrites. Ni-ferrite was determined to be the best suited for H_2 generation among the ferrites synthesized. The average H_2 cycle generated by $NiFe_2O_4$ was 0.442 cm^3/g. At the same temperature, Ni-ferrite H_2 productivity was substantially greater than other ferrites. They discovered that the crystal structure of $NiFe_2O_4$ did not change in repeated cycles during the redox reaction using XRD, and they concluded that $NiFe_2O_4$ is a structurally stable and durable material.

3. MATERIALS AND METHODS

3.1. Wind Turbine

Wind turbines are devices that transform the kinetic energy of air flowing from a high pressure area to a low pressure area first into mechanical energy, then into electrical energy. In the beginning, we mentioned wind turbine equipment. The rotor converts kinetic energy into mechanical energy when the wind rotates the turbine. The rotor shaft's rotating movement is accelerated and transmitted to the body's generator. The generator's electrical energy is stored in batteries or sent straight to the receivers. The wind turbine used is given in Figure 3.1 The blade length of the turbine is 1.5 m and the width is 0.26 m. PMSG generator diameter is 40 cm.

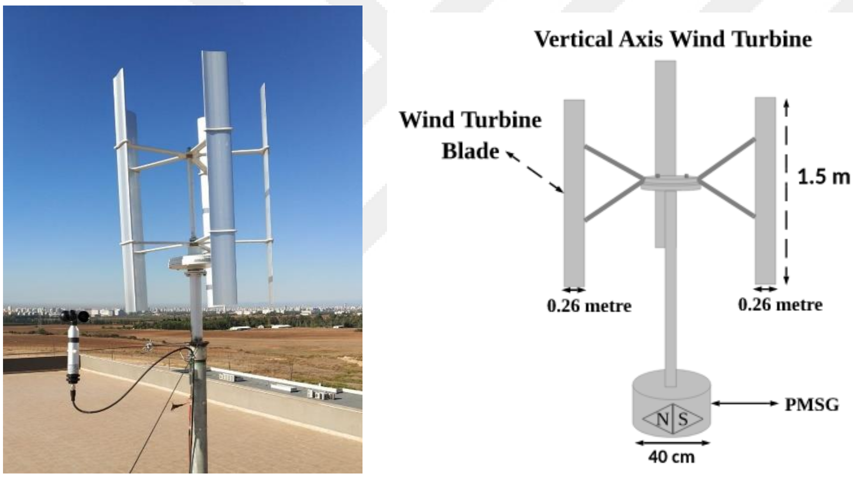

Figure 3.1. Vertical Axis Wind Turbine

In this study, vertical axis wind turbine and permanent magnet synchronous generator (PMSG) are used. PMSG is the most preferred generator type among synchronous generators in wind turbine applications. PMSG is widely used in wind turbine applications without the need for a gearbox because it is self-excited without the need for any energy source thanks to the permanent magnets in its rotor. Low-speed PMSGs have paved the way for more efficient wind turbines. Wind's erratic nature poses a challenge for traditional electric generators that must maintain a constant output. Permanent magnet generators can work at a variety of speeds, are lightweight due to their lack of gearing, and are extremely long-lasting. The fact that it can generate power at a high pace is its major benefit. Its biggest advantage is that it can generate power at any speed. Maintenance cost is low. It is suitable for small and light applications.

PMSG's stator is wound and permanent magnets are placed in its rotor. As seen in Figure 3.2, in this generator design, magnets are attached to the rotor surface with strong adhesives. Such structures are usually designed for low-speed applications so that the magnets do not become dislodged. Since the magnetic permeability of the magnets is close to the magnetic permeability of the air, the magnets also act like air, causing the air gap to be large.

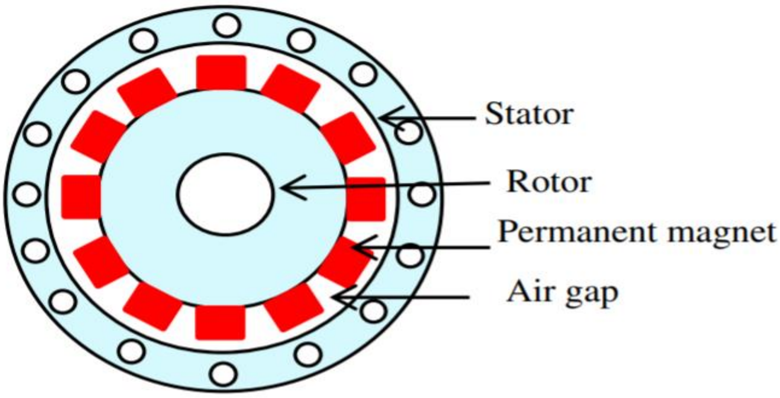

Figure 3.2. Permanent Magnet Synchronous Generator

3.2. Theoretical Power of Wind (Betz Law)

The theoretical power (Po) of the wind moving freely in the atmosphere was formulated by the German physicist Albert Betz based on the principles of conservation of kinetic energy and momentum as follows:

$$P_o = \frac{1}{2}\rho\, V_i^3 A\, C_p \tag{1}$$

Here, ρ is the air density (kg/m^3).

A is the cross-sectional area perpendicular to the direction of wind travel (m^2).

V represents the wind speed (m/sec).

C_p is the maximum power coefficient.

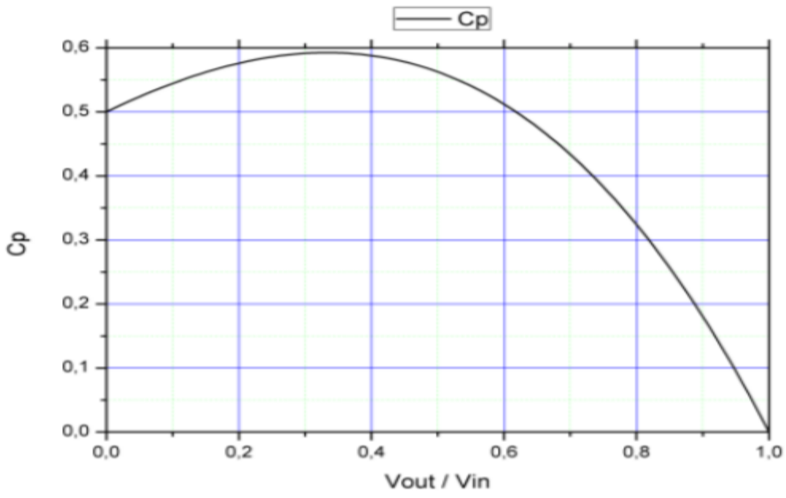

Figure 3.3. Efficiency for wind turbines

As can be seen in figure 3.3, it is seen that the maximum power coefficient occurs at the point where the V_O/V_i ratio is 1/3 and its value is 0.59. According to this equality, known as Betz's law, the maximum power that can be generated from a turbine;

$$P_o = \frac{1}{2}\rho\, V_i^3 A\ 0.59 \tag{1.1}$$

Betz's law theoretically states that the energy efficiency of a wind turbine will be 59% at the maximum. In other words, 59% of the kinetic energy of the wind can be used to spin the turbine and generate electricity. This situation, also known as Betz's law, is derived from the principle of conserving the momentum and mass of the air flow by means of a transmission disk that receives energy from the wind flow. According to this law, no turbine can use more than 0.59 percent of the kinetic energy in the wind. If the turbines could operate at full performance, they would have to collect all of the wind on themselves. In other words, it would be in the form of a solid closed disk so that no rotational movement would take place. If the wind on top of the turbine received all of its energy, the speed of the wind would drop to zero and no wind flow would be observed behind the turbine. For this reason, the maximum efficiency value that can be achieved with current technology becomes the Betz limit of 59%. Figure 3.4 shows the energy extracting stream-tube of a wind turbine.

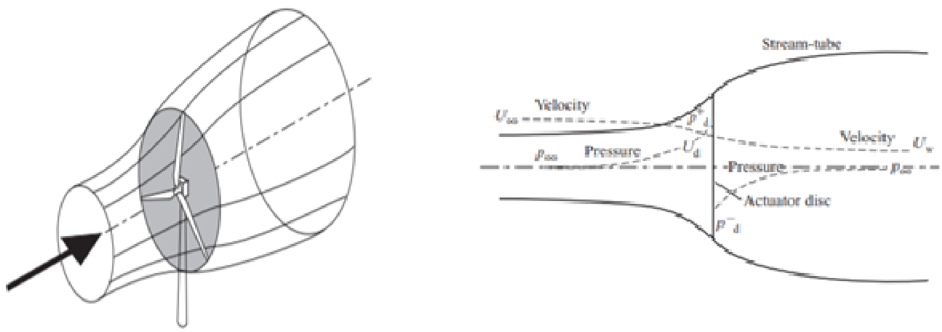

Figure 3.4. The Energy Extracting Stream-tube of a Wind Turbine

3.3. Forces forming the wind and affecting the wind speed

The generation of the wind and the flow of the wind need forces due to the shape of the earth. The pressure gradient force, centrifugal force, coriolis force, and friction force are all examples of these forces.

3.3.1. Pressure Gradient Force

The pressure gradient force is the force that causes air to push from a high-pressure location to a lower-pressure area. Thanks to this force, it contributes to the movement of air on the earth and to the formation of wind. The pressure gradient force is formalized as follows;

$$G = \frac{1}{\rho}\frac{\Delta P}{h} \quad (2)$$

Here, G; gradient force (atm),

ρ; air density (kg / m^3),

ΔP; pressure difference between isobars,

h; is the length between isobars.

As seen from the equation, the greater the pressure difference or the distance between the shorter the pressure gradient force will be stronger.

3.3.2. Coriolis Force

This force that causes the winds in the hemispheres to deviate in the opposite direction is called the coriolis force. It is a force resulting from the rotation of the earth on its axis. The Coriolis effect is vital in some industries. For example, in order for a missile or a shuttle launched into space to reach its destination and land properly, the Coriolis effect should also be included in the calculations and their orbits should be determined accordingly. Otherwise, millions of dollars of investments, a lot of effort and research will be lost in the space before they reach their goals.

Coriolis Force is formalized as follows;

$$f_{cor} = 2\Omega \sin\varphi \quad (3)$$

Here, f_c; Coriolis force,

Ω; the angular rotation speed of the earth (7292.10^{-5} rad s^{-1}),

φ; is the degree of latitude.

3.3.4. Centrifugal Force

Centrifugal force is the desire of objects around a rotating object to be thrown forward during this rotation. As the rotation speed increases and the radius of the rotation decreases, the effect of the centrifugal force increases. This force increases towards the equator and decreases towards the poles. This force is based on the force of gravity, the rotation of the earth around itself, and the inclination of the earth's axis.

Centrifugal Force is formalized as follows;

$$f_{cent} = mV^2 / R \quad (4)$$

Here, m; the acceleration of the centrifugal force acting on the unit mass (m/s^2),

V; wind speed (m/s),

R; It is expressed as the rotating diameter of the wind.

3.3.4. Frictional force

Frictional force is a factor that reduces its speed by the friction of winds to the Earth. In this way, it causes delay of movement or advancement in parts of the air layers that touch the ground, as well as complex movements such as turbulence in the air mass. The friction effect decreases as it rises from the ground. While the friction effect is not found on the seas, it is effective on the land. However, wind directions can also change due to friction.

3.4. Wind Turbine Data

Wind turbine data were taken on the roof of our school's engineering building. The voltage value produced by the turbine was taken at intervals of 10 minutes for 15 days in July. Only the maximum voltage values produced during the day are given in Table 3.1. As seen, the maximum voltage generated is approximately 20 V on the 14th day.

Table 3.1. Maximum voltage values produced by the wind turbine for 15 days.

Days	Max. Voltage Value (V)
1	17.295
2	17.970
3	15.110
4	19.061
5	19.589
6	16.270
7	17.469
8	16.301
9	16.516
10	19.618
11	19.990
12	18.919
13	19.561
14	19.999
15	17.481

3.5. Rectifier

Rectifier is the process of converting alternating current (AC) to direct current (DC). All rectifiers are made by connecting more than one diode together in a certain way to make the

AC to DC conversion process, which is possible with a single diode, more efficiently. The widely used full bridge rectifier circuit was used in our study.

3.5.1. Full Wave Bridge Rectifier

The waveforms of the Full Wave Bridge Rectifier circuit and input-output signals are shown in Figure 3.5. In the positive half-period of the input voltage, the diodes D2 and D4 will be in forward conduction and will act as closed switches, while D1 and D3 will act as open switches since they will be in the cutoff. Current will flow through the diodes D2 and D4, the load resistance will create a positive output voltage. In the negative half-period of the input voltage, diodes D1 and D3 will be in forward conduction and will act as closed switches, while D2 and D4 will act as open switches since they will be in the cutoff. The current will flow through the diodes D2 and D4, and the load resistance will similarly create a positive output voltage.

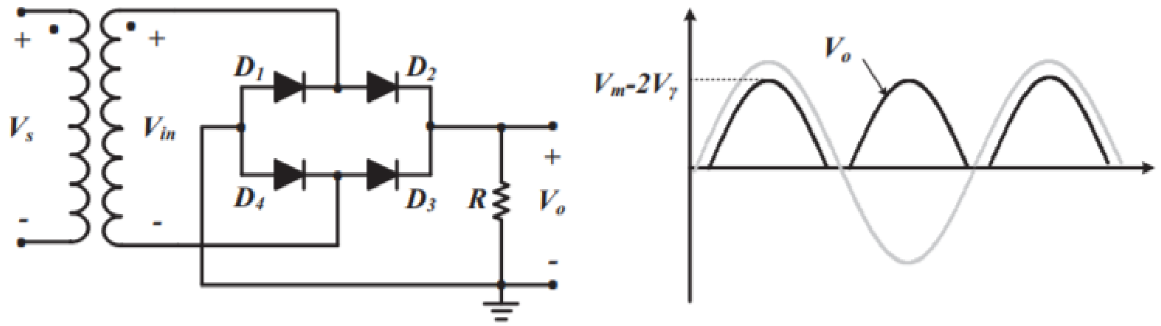

Figure 3.5. Full Wave Bridge Rectifier circuit and input-output voltage waveforms

Assuming the diodes are ideal, the DC output voltage of the full-wave rectifier is;

$$V_{0dc} = 2V_m / \pi \tag{5}$$

The DC output voltage of the full-wave rectifier will be equal to twice the DC output voltage of the half-wave rectifier.

3.5.2. Output Voltage Ripple and Filters

The most important point in power supplies is to minimize the voltage fluctuation of the rectified output. Filtering is done in order to reduce the ripple. In its simplest form, a filter circuit consists of a capacitor connected in parallel with the rectifier as seen in Figure 3.6.

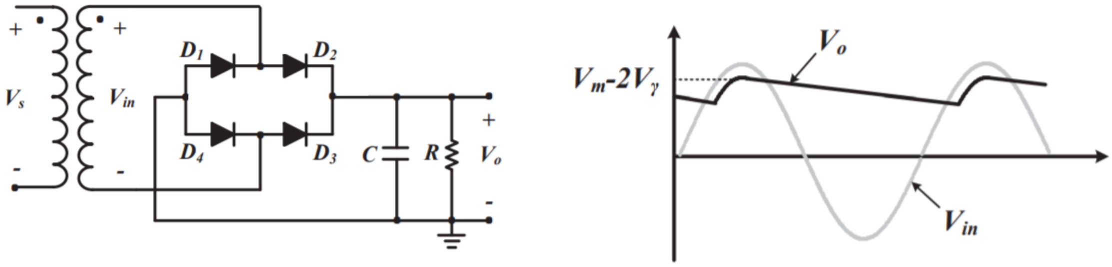

Figure 3.6. Full Wave Bridge rectifier circuit with Filter Capacitor and output waveform.

The waveforms of the Full Wave Bridge Rectifier circuit including the filter capacitor and the input-output signals are shown in Figure 3.6. If the diodes are considered ideal, the output voltage is;

$$Vodc = \frac{Vm}{1+\frac{1}{4fCR}} \tag{6}$$

The ripple seen in the output voltage;

$$Vr = \frac{V0dc}{fCR} \tag{7}$$

3.6. Buck Converter

A buck converter is a voltage-regulated converter that converts DC voltage to DC voltage at the output. The important thing is that the voltage you apply at the input must be higher than at the output. The purpose of using a buck converter in our system is to reach the low voltage we need for hydrogen production. The voltage obtained from the wind turbine has been reduced to the voltage levels we need with the help of the converter. The state of the switch on or off is the MOSFET used in the switch function. Figure 3.7 shows the on-state and off-state buck converter circuits.

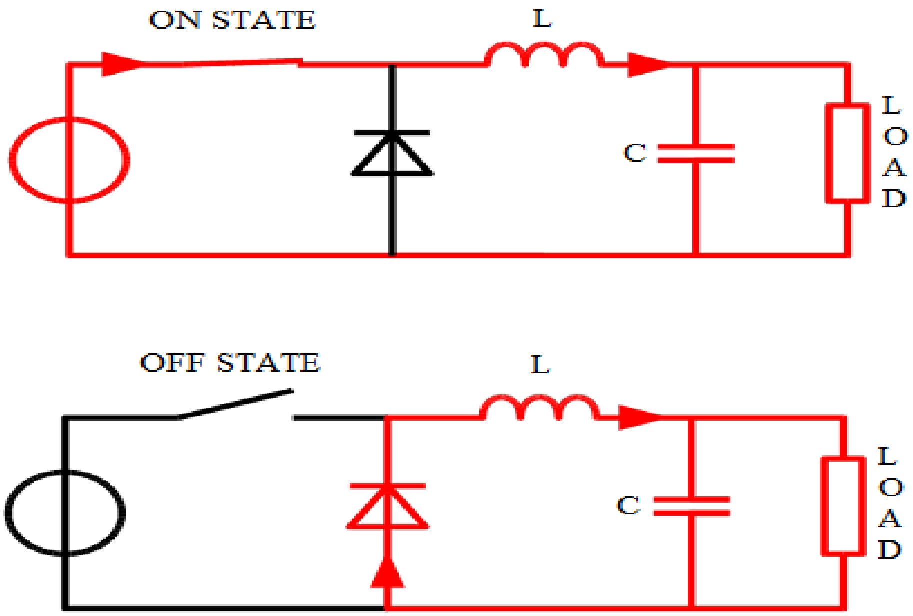

Figure 3.7. On-state and off-state buck converter circuit.

3.7. Voltage Divider

The voltage divider represents the amount of potential difference between two points, which is used to get a large voltage value and a small voltage value. It is one of the simple but frequently used applications that takes advantage of the effect of voltages falling on the components connected in series. We preferred to use resistant voltage divider in our study. We connected 3 series resistors and we reached the 3 V value we need. Thus, we had the opportunity to advance 3 different experiments simultaneously.

3.8. Modeling and Design

The highest voltage value we obtained as a result of the 15-day wind turbine experiment was approximately 20 V. In order to obtain the 3 V DC voltage required for our study, a module with wind turbine, DC-DC buck converter and voltage divider features was created and these parameters were simulated in the MATLAB/Simulink environment. The design I made is given in Figure 3.8.

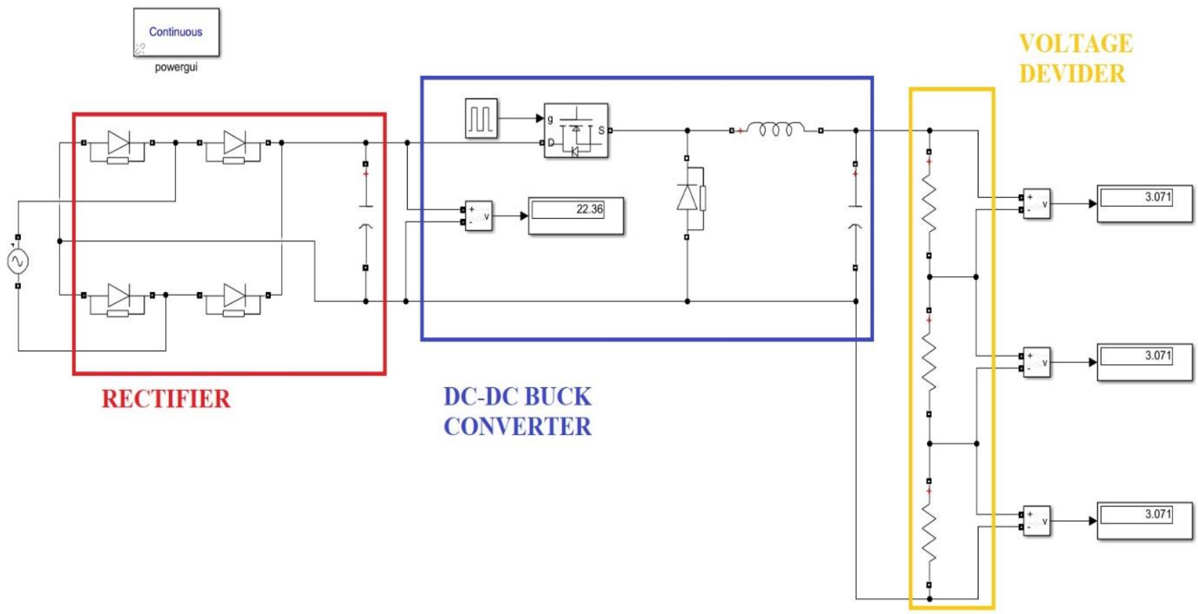

Figure 3.8. Wind turbine, rectifier, converter and voltage divider design in MATLAB/Simulink.

The experimental setup of the proposed system, which we simulated, was made. The schematic structure of the wind turbine assisted alkaline electrolysis system is shown in Figure 3.9. In this study, off grid system was preferred. The system is integrated into the electrolysis system. Thus, the AC voltage obtained from the wind turbine is converted to DC voltage with a rectifier, the voltage is reduced with a DC-DC buck converter, and finally, it is reduced to the desired voltage levels required for the electrolysis system with a voltage divider. Electrolysis was carried out with the energy from the wind turbine for hydrogen production. Excess energy was stored in the gel battery.

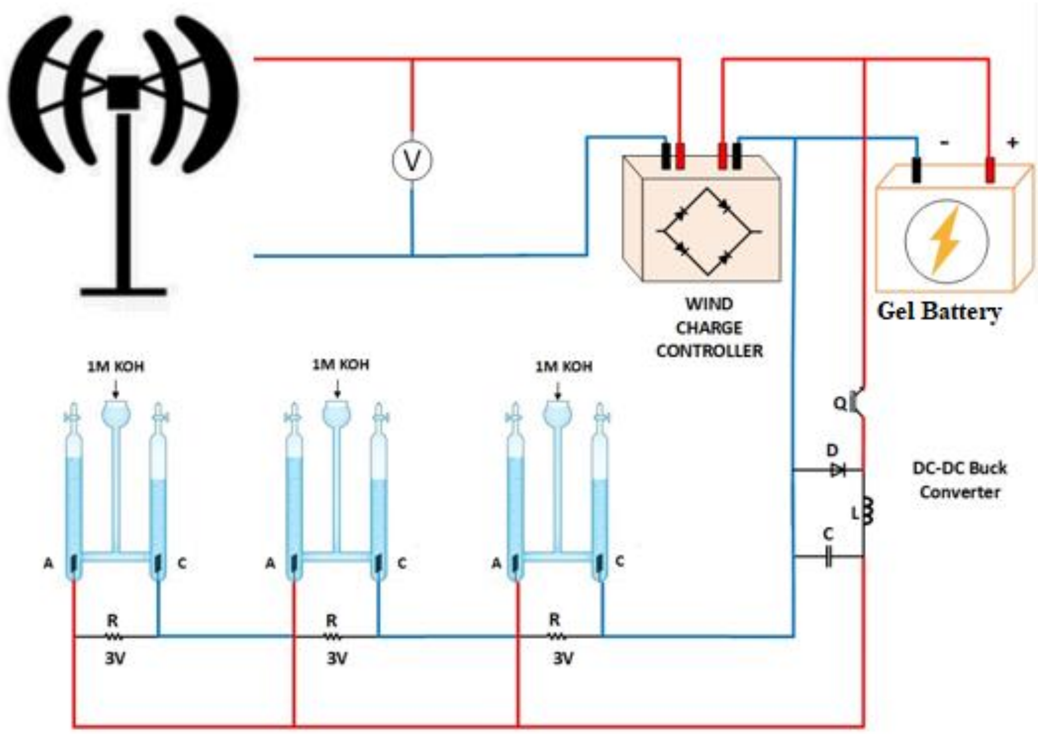

Figure 3.9. Wind turbine assisted alkaline electrolysis system.

3.9. Electrochemical Part

Graphite (G) electrode is preferred as cathode in our system due to its low cost. Copper wire was passed to one end of a graphite rod to provide conductivity. The electrode is 5 cm in length and embedded in polyester. The surface area of the prepared graphite electrode, which is not covered with resin in contact with the solution, is 0.36 cm^2. In Cell-1, a platinum (Pt) sheet with a surface area of 2 cm^2 was used as the anode electrode and graphite was used as the cathode. The stainless steel (SS), graphite (G) and copper (Cu) electrodes with a surface area of 0.78cm^2 were used as anode electrodes for other cells. Before the electrodeposition processes, the electrode surface was abraded up to 1200 degrees with sandpaper, except for the Pt electrode. Then, each electrode was washed with acetone/ethanol mixture and distilled water. Two electrode techniques were used for determining of decomposition voltages and produced gas volumes. The graphite cathode electrode was modified. The ternary coating was favored on graphite and Ni-Co-Cu was employed, based on the outstanding performance of binary coatings combining Ni-Co and Ni-Cu in the literature. Considering the literature, the coating's Co and Cu mole ratios should be kept low in comparison to the Ni mole ratio. The electrodeposition of nickel, cobalt, and copper was done galvanostatically with a three-electrode configuration on the Iviumstat Electrochemical Interface. Graphite was employed as the working electrode, nickel as the counter electrode, and an Ag/AgCl (3 M KCl) electrode as the reference electrode in this system. A coating thickness of 10 µm and a current density of 50 mA cm^{-2} were used. Chemical composition of coating baths are; nickel bath 30% $NiSO_4.7H_2O$, 1% $NiCl_2.6H_2O$, and 1.25% H_3BO_3; cobalt bath 30% $CoSO_4.7H_2O$, 1% $CoCl_2.6H_2O$, 1.25% H_3BO_3 ; copper bath 26.67% $CuSO_4.5H_2O$, 1.25% H_3BO_3. NiCoCu ternary coating was prepared by mixing in appropriate volumes to contain [Ni^{2+}], [Co^{2+}], [Cu^{2+}] ions at different concentrations in the plating bath. [Ni^{2+}]: [Co^{2+}]: [Cu^{2+}] mole ratio is 99 : 0.5 : 0.5.

Electrolysis was carried out using a direct current source and the amount of hydrogen produced both experimentally and theoretically at constant voltage. The theoretical calculations obtained by current-voltage curves with the help of Faraday Laws. A multimeter was used to determine the current flowing through the system. The cell components were given in Table 3.2.

Table 3.2. Working electrodes used in the electrolysis system in three different cells.

Cells	Anode	Cathode
Cell-1	Pt	G
Cell-2	SS	G
Cell-3	G	G
Cell-4	Cu	G
Cell-5	SS	G/NiCoCu
Cell-6	G	G/NiCoCu
Cell-7	Cu	G/NiCoCu

The minimum potential required for electrode reactions to start is called the decomposition voltage. The theoretical separation voltage can be found by calculating the electrode potentials corresponding to the equilibrium state of the anode and cathode with the Nernst equation. The theoretical decomposition voltage can be found by calculating the electrode potentials corresponding to the equilibrium state of the anode and cathode using the Nernst equation;

$$E_d = E_{anode} - E_{cathode} \quad (8)$$

The E_d obtained here is the theoretical decomposition voltage of the overvoltage at the anode and cathode. Theoretically, at 25 °C, the potential required for water to decompose is 1.23 V, where the evolution of hydrogen gas begins. (Yazıcı, 1995). However, a higher potential must be applied because of the over voltages caused by the solution and electrode metal and the internal resistance of the voltage source and the cables used during the experiment. During the electrolysis of alkaline water, oxygen is released at the anode and hydrogen gas at the cathode.

Anode : $4OH^- \rightarrow O_2 + 2H_2O + 4e^-$ E_A=0.401+0.0592pOH (PO_2=1.0 atm) (9)

Cathode: $4 H_2O + 4e^- \rightarrow 4OH^- + 2H_2$ E_C=-0.828+0.0592pOH (PH_2=1.0 atm) (10)

$2H_2O \rightarrow O_2 + 2H_2$ $E=E_A-E_C$=1.229 V (11)

The decomposition voltages in 1 M KOH solution were determined by using the stainless steel electrode at the anode and the graphite electrode at the cathode. For this purpose, the potential coming from the direct current source between 1.3 V and 3 V was applied to the system at 0.1 V intervals, and the current values passing through the system were determined and the current potential curves were obtained. Since the theoretical decomposition voltage is about 1.3 V, the studies were continued by starting with 1.3 V.

After the decomposition voltage was determined, hydrogen production volumes were observed at different voltage values. The amount of hydrogen production was investigated by placing the cathode, where the hydrogen gas output is, on the electrode by turning the cylinder upside down. The volume of hydrogen produced at all voltage values starting from 2.3 V and increasing by 0.1 V up to 3 V, and the current values passing through the system at each volt value were measured. Note the volume amounts displayed in the cylinder at 3-minute intervals at each volt. Each voltage value was applied to the system for 15 minutes. Considering that water vapor will also collect in the cylinder in the same environment, the volume correction was made as follows.

$$P_{H_2} = P_T - P_{H_2O} \tag{12}$$

When the vapor pressure of water (P_{H_2O}) under these conditions is 23.756 mmHg and the total atmospheric pressure (P_T) is 756 mmHg, the pressure of hydrogen (P_{H_2}) gas under these conditions is determined as 732.244 mmHg. Hydrogen volume (V_{H_2}) is;

$$V_{H_2} = \frac{732.244}{756} \text{ x } V_{measuring} \quad (13)$$

determined by the relation. The $V_{measuring}$ here is the total volume of gas collected experimentally in the cylinder.

3.10. Surface Characterization

An FEI Quanta 650 Field Emission SEM with an EDX detector was used to perform scanning electron microscopy (SEM) at 20 keV.

4. RESULT AND DISCUSSION

4.1. Hydrogen Production

Theoretically, the potential required for water decomposition at 25°C is 1.229 V. When the O_2 overvoltage (0.47 V) on Pt as the anode is added to this value, a potential of at least 1.70 V must be applied to the system to initiate the hydrogen gas evolution. The hydrogen gas was measured for the Cell-1 in 1 M KOH. Experimental decomposition voltage was calculated for each electrode in order to compare the volumes and the effectiveness of the coatings with each other. The decomposition voltage (E_d) for the Cell-1 electrode was 1.8 V and the overvoltage E_{over} was 0.5 V in Eq. 13.

$$E_{over} = E_d - 1.3 = 1.8 - 1.3 \quad (14)$$

$$E_{over} = 0.5 \text{ V}$$

Hydrogen production volumes of Cell-1 at different voltage values are given in Table 4.1. The graphite electrode and the platinum electrode are immersed in a 1 M KOH solution at a fixed distance of 2 cm. The burette was turned upside down and placed on the cathode side where the hydrogen gas escape was. Thus, the volume of the amount of hydrogen produced was measured. The experiments were obtained from 2.3 V to 3 V. As seen from Table 4.1 for 15 minutes at 3 V, hydrogen gas volume was 15 mL by using G cathode and Pt anode.

Table 4.1. Total charge (Q) during 15 minutes electrolysis, theoretical (V_t) and experimental (V_e) hydrogen volumes at the end of 15 minutes for various voltages (E) for G electrode in case of Cell-1.

E/V	Q (Coulomb)	V_t (mL)	V_e (mL)
2.3	39	4.54	3.50
2.4	50	5.79	4.75
2.5	63	7.29	6.25
2.6	73.5	8.54	7.50
2.7	86.5	1004	9.00
2.8	99.5	11.54	10.50
2.9	129.5	15.04	14.00
3.0	138	16.04	15.00

Different operation voltages and produced hydrogen gas volumes for each 3 minutes are given in Figure 4.1.

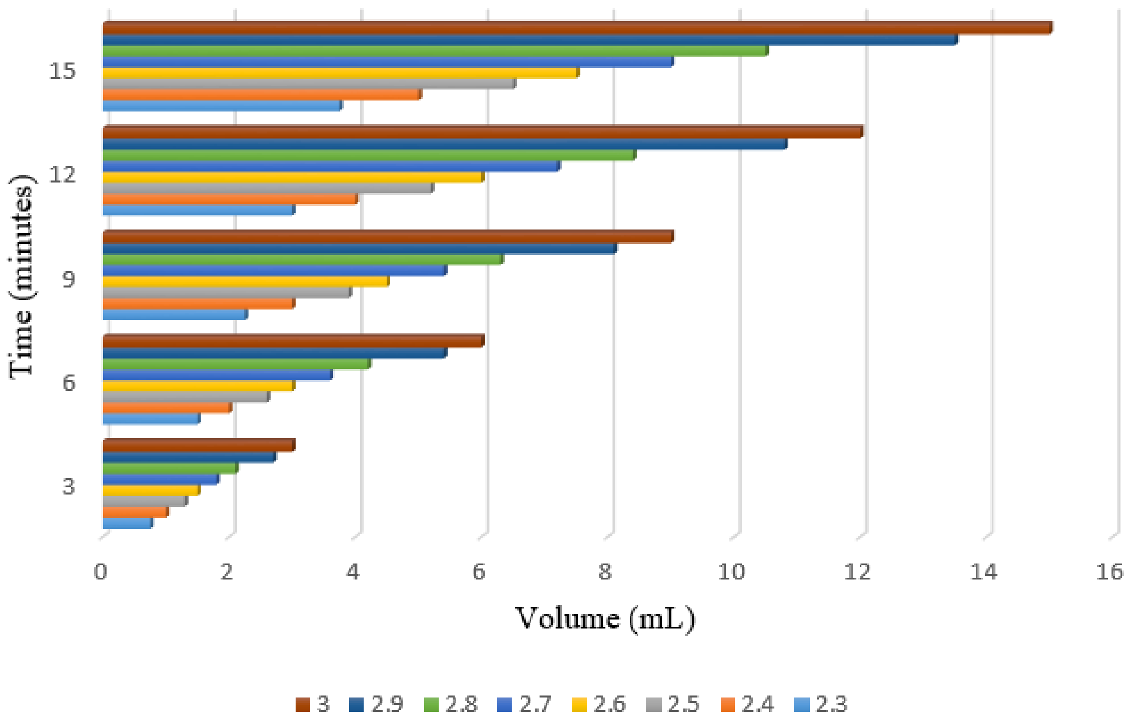

Figure 4.1. Amount of hydrogen volume value with G electrode from 2.3 V up to 3 V at each volt during the 15 minutes.

The hydrogen gas was measured for the Cell-2 in 1 M KOH. Experimental decomposition voltage was calculated for each electrode in order to compare the volumes and the effectiveness of the coatings with each other. The decomposition voltage (E_d) for the Cell-2 electrode was 1.9 V and the overvoltage E_{over} was 0.6V in Eq. 14.

$$E_{over} = E_d - 1.3 = 1.9 - 1.3 \quad (15)$$

$$E_{over} = 0.6\ V$$

Hydrogen production volumes of Cell-2 at different voltage values are given in Table 4.2. The experiments were obtained from 2.3 V to 3 V. As seen from Table 4.2 for 15 minutes at 3 V, hydrogen gas volume was 11.13 mL by using G cathode and SS anode.

Table 4.2. Total charge (Q) during 15 minutes electrolysis, theoretical (V_t) and experimental (V_e) hydrogen volumes at the end of 15 minutes for various voltages (E) for G electrode in case of Cell-2.

E/V	Q (coulomb)	V_t (mL)	V_e (mL)
2.3	23.88	2.77	2.42
2.4	33.48	3.88	3.58
2.5	56.52	6.56	6.30
2.6	65.16	7.56	7.26
2.7	74.52	8.65	8.13
2.8	82.8	9.61	9.20
2.9	88.36	10.26	10.16
3.0	97.74	11.34	11.13

Different operation voltages and produced hydrogen gas volumes for Cell-2 each 3 minutes are given in Figure 4.2.

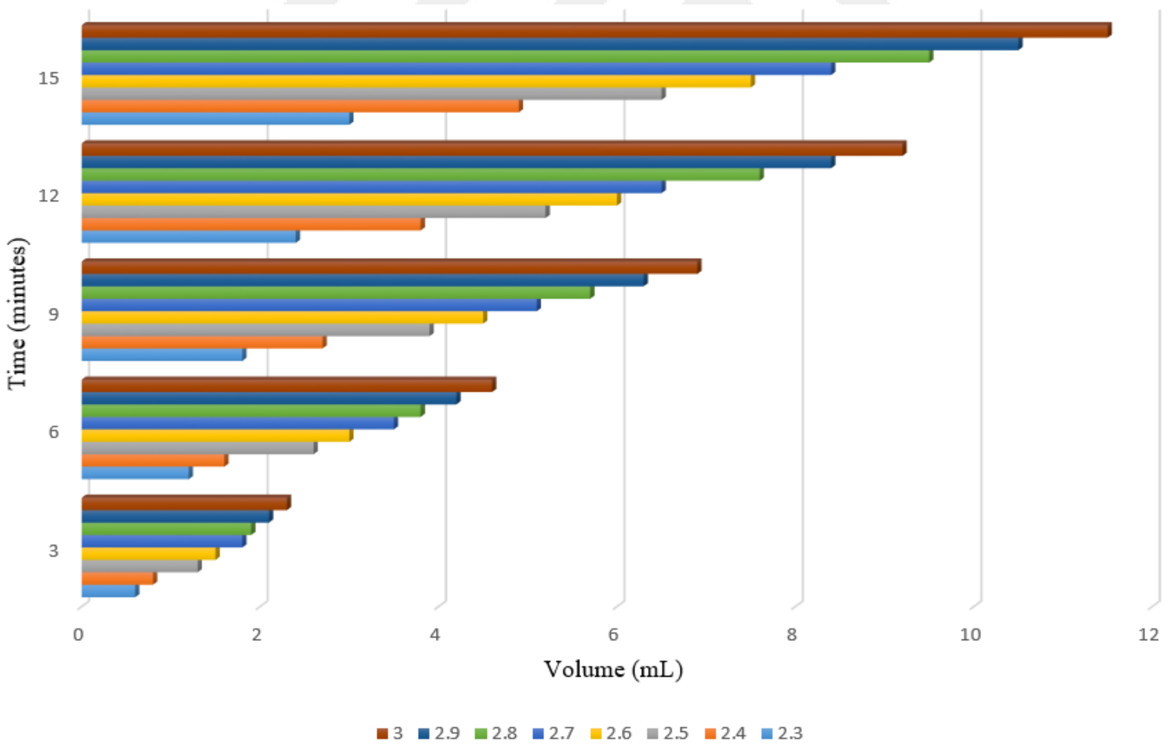

Figure 4.2. Amount of hydrogen volume value with G electrode from 2.3 V up to 3 V at each volt during the 15 minutes.

The hydrogen gas was measured for the Cell-3 in 1 M KOH. Experimental decomposition voltage was calculated for each electrode in order to compare the volumes and the effectiveness of the coatings with each other. The decomposition voltage (E_d) for the Cell-3 electrode was 2.0 V and the overvoltage E_{over} was 0.7 V in Eq. 15.

$$E_{over} = E_d - 1.3 = 2.0 - 1.3 \qquad (16)$$

$$E_{over} = 0.7 \text{ V}$$

Hydrogen production volumes of Cell-3 at different voltage values are given in Table 4.3. The experiments were obtained from 2.3 V to 3 V. As seen from Table 4.3 for 15 minutes at 3 V, hydrogen gas volume was 9.30 mL by using G cathode and G anode.

Table 4.3. Total charge (Q) during 15 minutes electrolysis, theoretical (V_t) and experimental (V_e) hydrogen volumes at the end of 15 minutes for various voltages (E) for G electrode in case of Cell-3.

E/V	Q (coulomb)	V_t (mL)	V_e (mL)
2.3	21.06	2.44	2.13
2.4	24.48	2.84	2.71
2.5	37.08	4.30	4.16
2.6	44.55	5.17	4.94
2.7	53.01	6.15	5.90
2.8	63.09	7.32	6.96
2.9	73.89	8.57	8.03
3.0	86.76	10.07	9.30

Different operation voltages and produced hydrogen gas volumes for Cell-3 each 3 minutes are given in Figure 4.3.

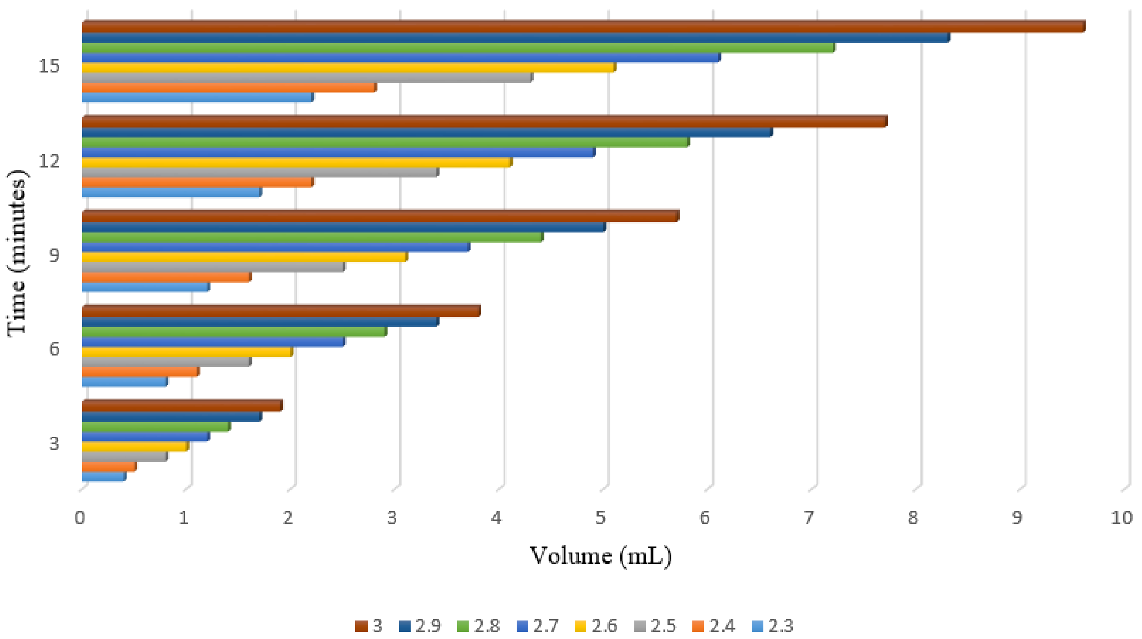

Figure 4.3. Amount of hydrogen volume value with G electrode from 2.3 V up to 3 V at each volt during the 15 minutes.

The hydrogen gas was measured for the Cell-4 in 1 M KOH. Experimental decomposition voltage was calculated for each electrode in order to compare the volumes and the effectiveness of the coatings with each other. The decomposition voltage (E_d) for the Cell-4 electrode was 2.1 V and the overvoltage E_{over} was 0.8 V in Eq. 16.

$$E_{over} = E_d - 1.3 = 2.1 - 1.3 \quad (17)$$

$$E_{over} = 0.8 \text{ V}$$

Hydrogen production volumes of Cell-4 at different voltage values are given in Table 4.4. The experiments were obtained from 2.3 V to 3 V. As seen from Table 4.4 for 15 minutes at 3 V, hydrogen gas volume was 8.71 mL by using G cathode and Cu anode.

Table 4.4. Total charge (Q) during 15 minutes electrolysis, theoretical (V_t) and experimental (V_e) hydrogen volumes at the end of 15 minutes for various voltages (E) for G electrode in case of Cell-4.

E/V	Q (coulomb)	V_t (mL)	V_e (mL)
2.3	25.20	2.92	2.80
2.4	33.03	3.83	3.48
2.5	42.03	4.88	4.35
2.6	49.32	5.72	5.13
2.7	55.53	6.44	5.90
2.8	63.63	7.38	6.67
2.9	71.19	8.26	7.74
3.0	79.47	9.22	8.71

Different operation voltages and produced hydrogen gas volumes for Cell-4 each 3 minutes are given in Figure 4.4.

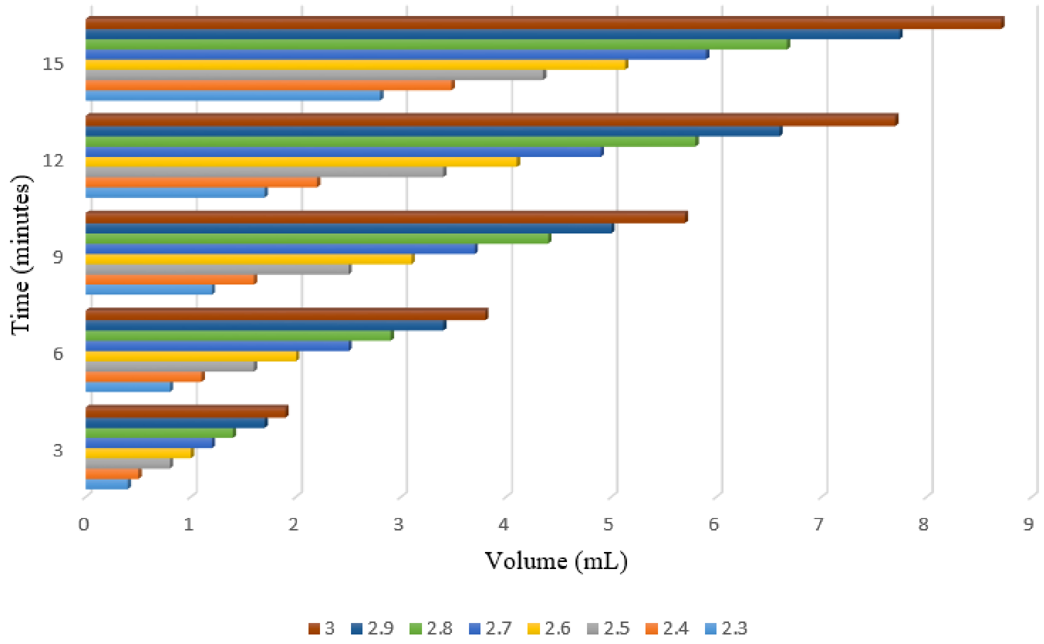

Figure 4.4. Amount of hydrogen volume value with G electrode from 2.3 V up to 3 V at each volt during the 15 minutes.

The hydrogen gas was measured for the Cell-5 in 1 M KOH. Experimental decomposition voltage was calculated for each electrode in order to compare the volumes and the effectiveness of the coatings with each other. The decomposition voltage (E_d) for the Cell-5 electrode was 1.85 V and the overvoltage E_{over} was 0.55 V in Eq. 17.

$$E_{over} = E_d - 1.3 = 1.85 - 1.3 \quad (18)$$

$$E_{over} = 0.55 \text{ V}$$

Hydrogen production volumes of Cell-5 at different voltage values are given in Table 4.5. The experiments were obtained from 2.3 V to 3 V. As seen from Table 4.5 for 15 minutes at 3 V, hydrogen gas volume was 13.12 mL by using G/NiCoCu cathode and SS anode.

Table 4.5. Total charge (Q) during 15 minutes electrolysis, theoretical (V_t) and experimental (V_e) hydrogen volumes at the end of 15 minutes for various voltages (E) for G/NiCoCu electrode in case of Cell-5.

E/V	Q (Coulomb)	V_t (mL)	V_e (mL)
2.3	52.83	6.14	5.94
2.4	67.68	7.86	7.60
2.5	73.98	8.60	8.30
2.6	84.42	9.80	9.48
2.7	91.26	10.60	10.25
2.8	99.63	11.56	11.20
2.9	107.73	12.50	12.10
3.0	116.82	13.56	13.12

Different operation voltages and produced hydrogen gas volumes for Cell-5 each 3 minutes are given in Figure 4.5.

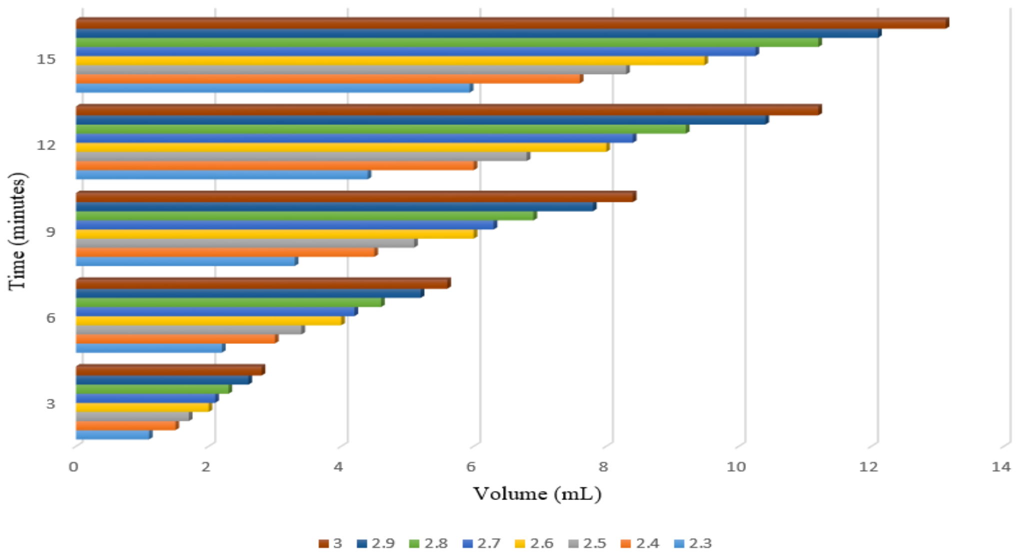

Figure 4.5. Amount of hydrogen volume value with G/NiCoCu electrode from 2.3 V up to 3 V at each volt during the 15 minutes.

The hydrogen gas was measured for the Cell-6 in 1 M KOH. Experimental decomposition voltage was calculated for each electrode in order to compare the volumes and the effectiveness of the coatings with each other. The decomposition voltage (E_d) for the Cell-6 electrode was 1.95 V and the overvoltage E_{over} was 0.65 V in Eq. 18.

$$E_{over} = E_d - 1.3 = 1.95 - 1.3 \quad (19)$$

$$E_{over} = 0.65 \text{ V}$$

Hydrogen production volumes of Cell-6 at different voltage values are given in Table 4.6. The experiments were obtained from 2.3 V to 3 V. As seen from Table 4.6 for 15 minutes at 3 V, hydrogen gas volume was 10.10 mL by using G/NiCoCu cathode and G anode.

Table 4.6. Total charge (Q) during 15 minutes electrolysis, theoretical (V_t) and experimental (V_e) hydrogen volumes at the end of 15 minutes for various voltages (E) for G/NiCoCu electrode in case of Cell-6.

E/V	Q (Coulomb)	Vt (mL)	Vd (mL)
2.3	36.54	4.24	4.11
2.4	45.0	5.22	5.06
2.5	50.67	5.88	5.69
2.6	56.52	6.56	6.35
2.7	65.34	7.58	7.34
2.8	71.46	8.29	8.03
2.9	80.1	9.30	9.00
3.0	89.82	10.42	10.10

Different operation voltages and produced hydrogen gas volumes for Cell-6 each 3 minutes are given in Figure 4.6.

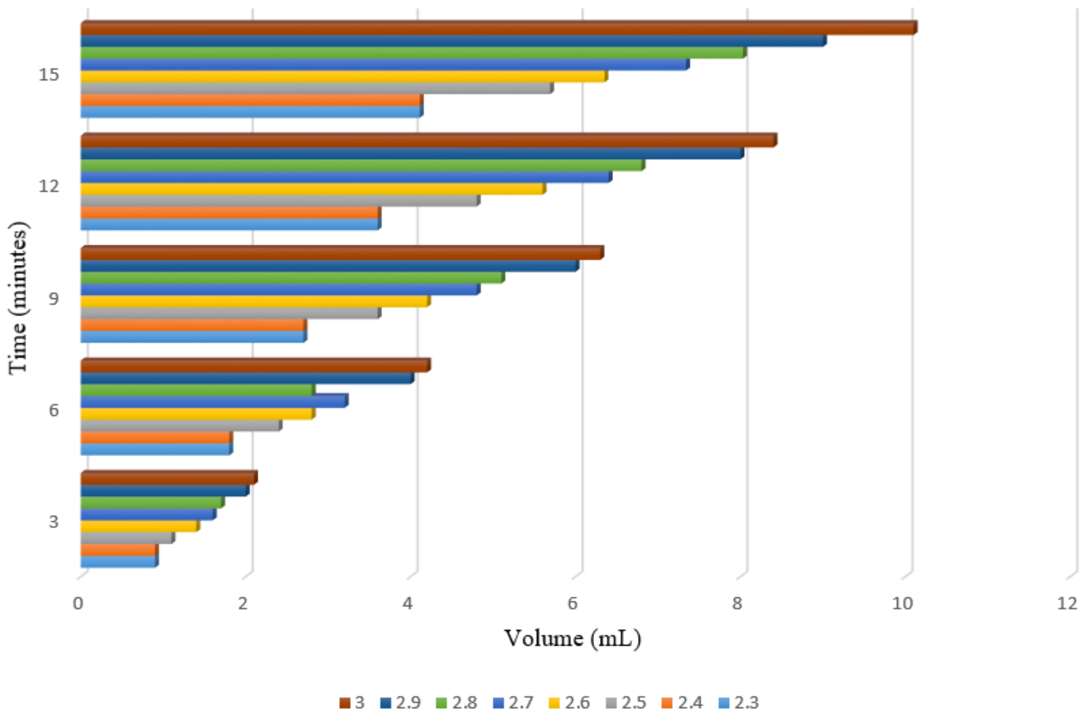

Figure 4.6. Amount of hydrogen volume value with G/NiCoCu electrode from 2.3 V up to 3 V at each volt during the 15 minutes.

The hydrogen gas was measured for the Cell-7 in 1 M KOH. Experimental decomposition voltage was calculated for each electrode in order to compare the volumes and the effectiveness of the coatings with each other. The decomposition voltage (E_d) for the Cell-7 electrode was 1.97 V and the overvoltage E_{over} was 0.67 V in Eq. 19.

$$E_{over} = E_d - 1.3 = 1.97 - 1.3 \quad (20)$$

$$E_{over} = 0.67 \text{ V}$$

Hydrogen production volumes of Cell-7 at different voltage values are given in Table 4.7. T The experiments were obtained from 2.3 V to 3 V. As seen from Table 4.7 for 15 minutes at 3 V, hydrogen gas volume was 10.97 mL by using G/NiCoCu cathode and Cu anode.

Table 4.7. Total charge (Q) during 15 minutes electrolysis, theoretical (V_t) and experimental (V_e) hydrogen volumes at the end of 15 minutes for various voltages (E) for G/NiCoCu electrode in case of Cell-7.

E/V	Q (Coulomb)	Vt (mL)	Vd (mL)
2.3	41.22	4.78	4.64
2.4	50.94	5.91	5.72
2.5	60.12	6.98	6.75
2.6	63.00	7.31	7.08
2.7	71.19	8.26	8.00
2.8	83.25	9.66	9.35
2.9	89.62	10.42	10.10
3.0	97.65	11.33	10.97

Different operation voltages and produced hydrogen gas volumes for Cell-7 each 3 minutes are given in Figure 4.7.

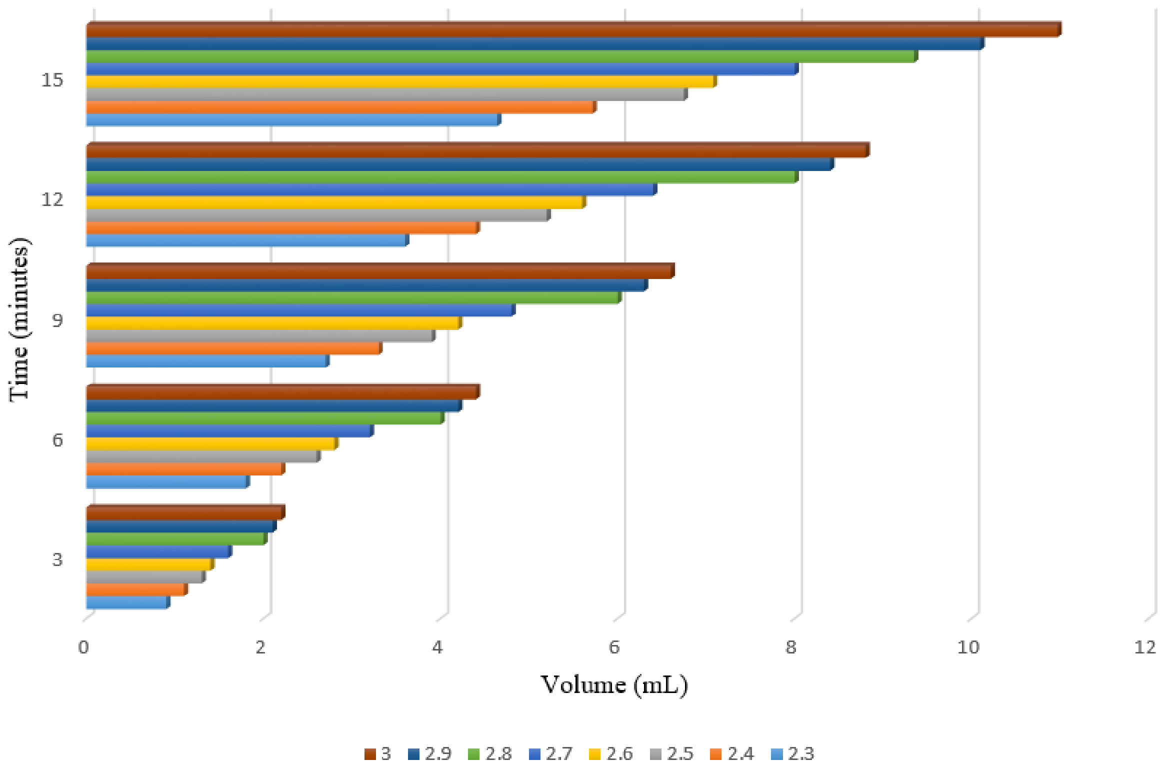

Figure 4.7. Amount of hydrogen volume value with G/NiCoCu electrode from 2.3 V up to 3 V at each volt during the 15 minutes.

Scanning electron microscope is a type of electron microscope that obtains an image by scanning the surface of the sample to be examined with an electron beam. Electrons interact with atoms in the sample to produce different signals containing information about the sample surface. Secondary electrons emitted by sample atoms excited by the electron beam are mostly used to create images in SEM. The change in the number of secondary electrons ejected from different parts of the sample primarily depends on the angle of encounter of the beam with the surface, that is, on the topography of the surface. Secondary electrons scattered from the surface atoms provide information about the sample surface, while backscattered electrons are used to detect fundamental differences in the sample surface through the contrast difference between regions with different chemical compositions.

4.2. Surface Characterization

The structure of the NiCoCu coating generated on the surface of the graphite electrode employed in the study was studied using SEM and EDX images. The homogenous lobulated shapes were detercted on the surface of G/NiCoCu electrode. As seen in Figure 4.8, homogeneous lobulated shapes were detected on the G/NiCoCu electrode surface.

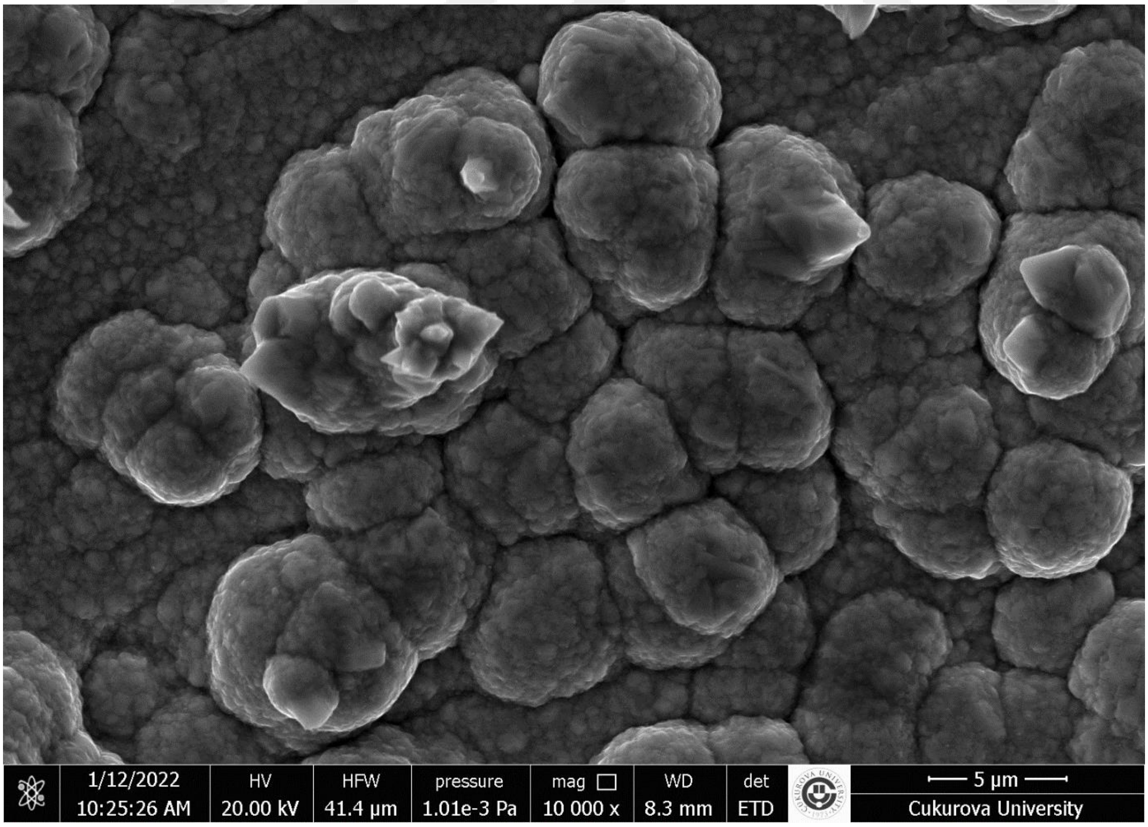

Figure 4.8. The SEM micrograph of G/NiCoCu surface

EDX mapping analysis was given in Figure 4.9. On the electrode surface, all atoms were uniformly deposited. As seen in Table 4.8, the weight percent of Ni, Co, Cu were 95.09, 2.22 and 2.69%, respectively.

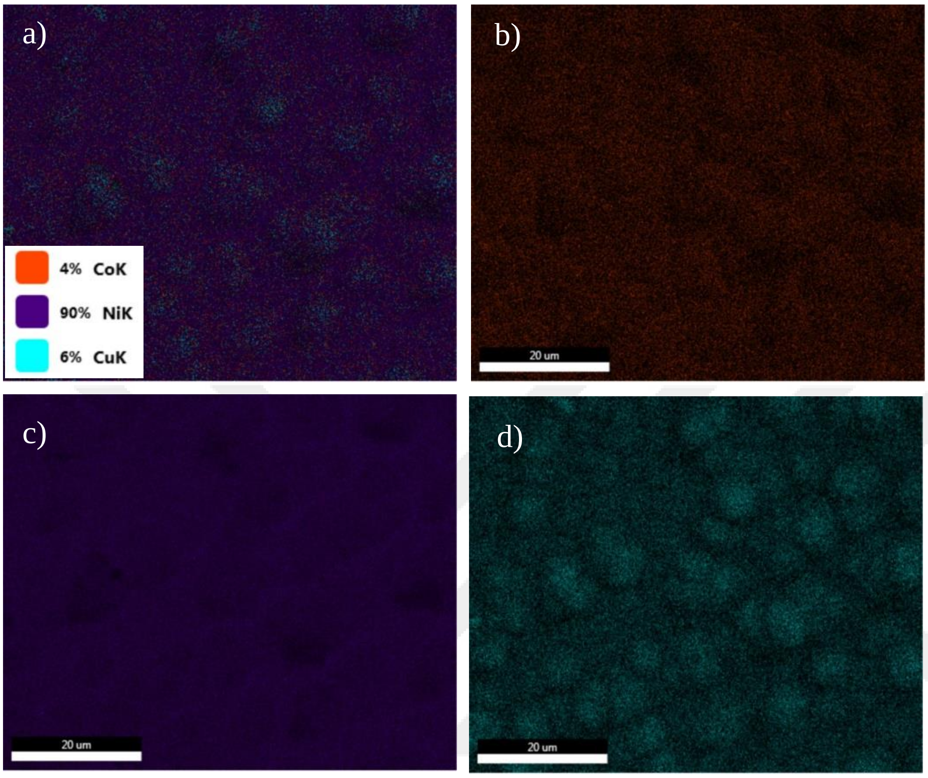

Figure 4.9. EDX mapping of G/NiCoCu (a); Co red dot (b); Ni purple dot (c) and Cu green dot (d)

Table 4.8. EDX analysis, the percent values of Ni, Co, Cu elements

Elements	%
Ni	95.09
Co	2.22
Cu	2.69

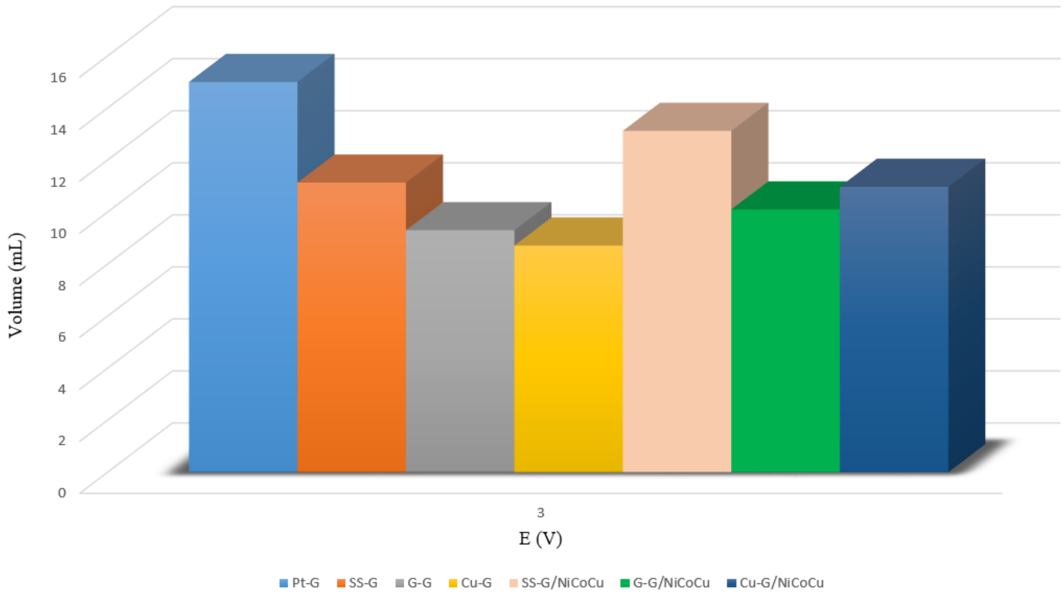

Figure 4.10. Comparison of hydrogen production amounts of Pt-G, SS-G, G-G, Cu-G, SS-G/NiCoCu, G-G/NiCoCu, Cu-G/NiCoCu and electrodes after 15 minutes at 3V.

Hydrogen production of each cell was observed with a graduated cylinder filled with 1 M KOH electrolyte. Pt-G (Cell-1), SS-G (Cell-2), GG (Cell-3), Cu-G (Cell-4), SS-G/NiCoCu (Cell-5), GG/NiCoCu (Cell-6) and Cu-G/NiCoCu (Cell-7) hydrogen performance are compared in Figures 4.10. In this study, 15 mL, 11.13 mL, 9.30 mL, 8.71 mL, 13.12 mL, 10.10 mL and 10.97 mL hydrogen gas were produced for 15 minutes, respectively, by applying 3 V. Although Cell-1 had the highest hydrogen production values at higher potentials (2.9 V and 3 V), Cell-5 was more suitable for lower potentials (2.3 V to 2.8 V). As a result, in the range of 2.3 V and 2.8 V, the modified cathode (G/NiCoCu) increased the catalytic activity.

5. CONCLUSIONS

In this study, wind energy assisted hydrogen production was investigated. For this purpose, vertical wind turbine with permanent magnet synchronous generator (PMSG) was used. The produced voltage values were determined during 15 days with 10 minutes intervals. The system was theoretically design via MATLAB/Simulink. In the electrolysis cell, graphite electrode was preferred as the cathode electrode because of its low cost. Hydrogen productions of various electrodes between 2.3 V and 3 V were examined. The Pt, SS, G and Cu electrodes were used as anode, G electrode was used as cathode. Results showed that, produced hydrogen gas values were 15 mL; 11.13 mL, 9.30 mL and 8.71 at 3V for 15 minutes electrolysis period, by using Pt-G (Cell-1); SS-G (Cell-2); G-G(Cell-3) and Cu-G (Cell-4) respectively.

Then, the G electrode was modified using ternary coating (Ni, Co and Cu). The performance of G/NiCoCu cathode was tested versus SS, G and Cu anodes. The results showed that, produced hydrogen gas values were 13.12 mL; 10.10 mL and 10.97 at 3V for 15 minutes electrolysis period, by using SS-G/NiCoCu (Cell-5); G-G/NiCoCu (Cell-6) and Cu-G/NiCoCu(Cell-7) respectively. The Cell-5 exhibited better efficiency than other electrodes from 2.3 V to 2.8 V. Considering the results, we recommend the SS anode for hydrogen production both in terms of cost and corrosion resistance, and the SS-G/NiCoCu electrode due to its high hydrogen evolution performance, especially at low potentials. Cell-5 was observed to be the optimal setup for alkaline electrolysis compared to whole cells.

6. RECOMMENDATIONS

Due to the increasing population rate of our world and its interest in industrialization, the demand for energy continues to pollute the environment by increasing day by day. In order to leave a livable green world in better conditions for future generations after us, countries should invest in renewable energy sources without wasting time. Turkey is a country with high foreign dependency to meet its energy needs. Renewable energy sources can save the Turkish economy from the narrow economy it is in and reduce foreign dependency. The physical-geographical location of our country is very suitable for renewable energy production, and it is in a very productive position especially in terms of geothermal, solar and wind energy. These positions should be supported with government incentives.

Looking at the literature, it is seen that the energy carrier hydrogen will reach an important point in the near future. Studies in this area should be increased and new cathode materials should be produced. Thus, its cost will decrease and it will get the position it deserves. We recommend that the Cell-5 could be an attractive alternative in alkaline electrolysis system assisted by clean energy generated from wind energy for hydrogen production. It will be convenient on grid alternative renewable sources (PV, wind) supported industrial scale systems. If we want to achieve our goal of zero carbon emissions in 2050, cleaner and more reliable energies must be produced by integrating each other renewable energy sources (wind, hydrogen, solar, etc.).

REFERENCES

Akpınar, A., Kömürcü, M. İ., Kankal, M., Özölçer, İ. H., & Kaygusuz, K. (2008). Energy situation and renewables in Turkey and environmental effects of energy use. *Renewable and Sustainable Energy Reviews*, *12*(8), 2013-2039.

An, L., Feng, J., Zhang, Y., Wang, R., Liu, H., Wang, G. C., ... & Xi, P. (2019). Epitaxial heterogeneous interfaces on N-NiMoO4/NiS2 nanowires/nanosheets to boost hydrogen and oxygen production for overall water splitting. *Advanced Functional Materials*, *29*(1), 1805298.

Bhosale, R., Khadka, R., Puszynski, J., & Shende, R. (2011). H2 generation from two-step thermochemical water-splitting reaction using sol-gel derived SnxFeyOz. *Journal of Renewable and Sustainable Energy*, *3*(6), 063104.

Chen, H., Lv, E., Ji, Q., Zou, L., Liu, H., Yong, J., & Gao, J. (2020). Bimetallic metal–organic framework-derived carbon nanocubes as efficient electrocatalysts for oxygen evolution reaction. *Journal of Solid State Chemistry*, *291*, 121679.

Chowdhury, M. M., Haque, M. E., Das, D., Gargoom, A., & Negnevitsky, M. (2015). Modeling, parameter measurement and sensorless speed estimation of IPM synchronous generator for direct drive variable speed wind turbine application. *International Transactions on Electrical Energy Systems*, *25*(9), 1814-1830.

David, T. M., Wilson, P., Mahesh, R., Sagayaraj, P., Murugesan, N., Ramesh, C., & Seshadri, H. (2018). Photocatalytic water splitting of TiO2 nanotubes powders prepared via rapid breakdown anodization sensitized with Pt, Pd and Ni nanoparticles. *Materials technology*, *33*(4), 288-300.

De Fátima Palhares, D. D. A., Vieira, L. G. M., & Damasceno, J. J. R. (2018). Hydrogen production by a low-cost electrolyzer developed through the combination of alkaline water electrolysis and solar energy use. *International Journal of Hydrogen Energy*, *43*(9), 4265-4275.

Demirol, M., & Demirol, T. N. Rüzgar Elektrik Santrallerinin Şebeke Bağlantı Analizleri İçin Simülasyon Modelinin Oluşturulması. *Gazi Mühendislik Bilimleri Dergisi (Gmbd), 1*(3), 351-368.

Du, L., Sun, Y., & You, B. (2021). Hybrid water electrolysis: Replacing oxygen evolution reaction for energy-efficient hydrogen production and beyond. *Materials Reports: Energy*, *1*(1), 100004.

Erdoğan, N. (2020). *Türkiye'de Yenilenebilir Enerjiye Yönelik Teşvikler İle Yenilenebilir Enerji Üretimi Arasındaki Etkileşim Ve Finansal Yansımaları (Master's thesis, Sivas Cumhuriyet Üniversitesi-Sosyal Bilimler Enstitüsü)* (Doctoral dissertation, Yüksek Lisans Tezi. Sivas: Cumhuriyet Üniversitesi, Sosyal Bilimler Enstitüsü).

Feng, L. L., Yu, G., Wu, Y., Li, G. D., Li, H., Sun, Y., ... & Zou, X. (2015). High-index faceted Ni3S2 nanosheet arrays as highly active and ultrastable electrocatalysts for water splitting. *Journal of the American Chemical Society*, *137*(44), 14023-14026.

Genç, M. S., Çelik, M., & Karasu, İ. (2012). A review on wind energy and wind–hydrogen production in Turkey: A case study of hydrogen production via electrolysis system supplied by wind energy conversion system in Central Anatolian Turkey. *Renewable and sustainable energy reviews*, *16*(9), 6631-6646.

Gu, X., Liu, Z., Liu, H., Pei, C., & Feng, L. (2021). Fluorination of ZIF-67 framework templated Prussian blue analogue nano-box for efficient electrochemical oxygen evolution reaction. *Chemical Engineering Journal*, *403*, 126371.

Han, S. B., Kang, T. B., Joo, O. S., & Jung, K. D. (2007). Water splitting for hydrogen production with ferrites. *Solar Energy*, *81*(5), 623-628.

Ishaq, H., Dincer, I., & Naterer, G. F. (2018). Development and assessment of a solar, wind and hydrogen hybrid trigeneration system. *International Journal of Hydrogen Energy*, *43*(52), 23148-23160.

Jiang, H., Zhang, K., Li, W., Cui, Z., He, S. A., Zhao, S., ... & Brett, D. J. (2020). MoS2/NiS core-shell structures for improved electrocatalytic process of hydrogen evolution. *Journal of Power Sources*, *472*, 228497.

Jiang, J., Zhu, L., Sun, Y., Chen, Y., Chen, H., Han, S., & Lin, H. (2019). Fe2O3 nanocatalysts on N-doped carbon nanomaterial for highly efficient electrochemical hydrogen evolution in alkaline. *Journal of Power Sources*, *426*, 74-83.

Jiang, L., Yang, N., Yang, C., Zhu, X., Jiang, Y., Shen, X., ... & Sun, Q. (2020). Surface wettability engineering: CoSx-Ni3S2 nanoarray electrode for improving overall water splitting. *Applied Catalysis B: Environmental*, *269*, 118780.

Jafari, T., Moharreri, E., Amin, A. S., Miao, R., Song, W., & Suib, S. L. (2016). Photocatalytic water splitting—the untamed dream: a review of recent advances. *Molecules, 21*(7), 900.

Jurasz, J., Canales, F. A., Kies, A., Guezgouz, M., & Beluco, A. (2020). A review on the complementarity of renewable energy sources: Concept, metrics, application and future research directions. *Solar Energy*, *195*, 703-724.

Koç, A. , Yağlı, H. , Koç, Y. & Uğurlu, İ. (2018). Dünyada ve Türkiye'de Enerji Görünümünü n Genel Değerlendirilmesi. *Mühendis ve Makina* , 59 (692) , 86-114 .

Koç, E., Şenel, M. C. 2013. "Dünyada ve Türkiye'de Enerji Durumu - Genel Değerlendirme," *Mühendis ve Makina*, cilt 54, sayı 639, s. 32-44.

Krishnan, A., Aswani, J., Syamli, S., Nayar, S., & Shibli, S. M. A. (2020). Titanium dioxide decorated polyaniline nanocomposite induced photo catalytic water splitting reaction for hydrogen generation. *Materials Today: Proceedings*, *33*, 1277-1282.

Lai, B., Singh, S. C., Bindra, J. K., Saraj, C. S., Shukla, A., Yadav, T. P., ... & Guo, C. (2019). Hydrogen evolution reaction from bare and surface-functionalized few-layered MoS2 nanosheets in acidic and alkaline electrolytes. *Materials Today Chemistry*, *14*, 100207.

Landman, A., Halabi, R., Dias, P., Dotan, H., Mehlmann, A., Shter, G. E., ... & Rothschild, A. (2020). Decoupled photoelectrochemical water splitting system for centralized hydrogen production. *Joule*, *4*(2), 448-471.

Li, J., Shen, P. K., & Tian, Z. (2017). One-step synthesis of Ni3S2 nanowires at low temperature as efficient electrocatalyst for hydrogen evolution reaction. *International Journal of Hydrogen Energy*, *42*(10), 7136-7142.

Liao, C. H., Huang, C. W., & Wu, J. (2012). Hydrogen production from semiconductor-based photocatalysis via water splitting. *Catalysts*, *2*(4), 490-516.

Liu, Z., Jiang, J., Liu, Y., Huang, G., Yuan, S., Li, X., & Li, N. (2021). Boosted hydrogen evo lution reaction based on synergistic effect of RuO2@ MoS2 hybrid electrocatalyst. *Applied Su rface Science*, *538*, 148019.

Ma, L., Zhang, K., Wang, S., Gao, L., Sun, Y., Liu, Q., ... & Zhang, X. (2019). Vanadium doping over Ni3S2 nanosheet array for improved overall water splitting. *Applied Surface Science*, *489*, 815-823.

Manabe, A., Kashiwase, M., Hashimoto, T., Hayashida, T., Kato, A., Hirao, K., ... & Nagashima, I. (2013). Basic study of alkaline water electrolysis. *Electrochimica Acta*, *100*, 249-256.

Mert, M. E., Mert, B. D., Kardaş, G., & Yazıcı, B. (2017). The photoelectrocatalytic activity, long term stability and corrosion performance of NiMo deposited titanium oxide nano-tubes for hydrogen production in alkaline medium. *Applied Surface Science*, *423*, 704-715.

Nemiwal, M., Gosu, V., Zhang, T. C., & Kumar, D. (2021). Metal organic frameworks as electrocatalysts: Hydrogen evolution reactions and overall water splitting. *International Journal of Hydrogen Energy*.

Ni, M., Leung, M. K., Leung, D. Y., & Sumathy, K. (2007). A review and recent developments in photocatalytic water-splitting using TiO2 for hydrogen production. *Renewable and Sustainable Energy Reviews*, *11*(3), 401-425.

Ng, K. H., Yuan, L. S., Cheng, C. K., Cheng, Y. W., & Chong, C. C. (2021). Photocatalytic water splitting for solving energy crisis: Myth, Fact or Busted?. *Chemical Engineering Journal*, 128847.

Olateju, B., & Kumar, A. (2011). Hydrogen production from wind energy in Western Canada for upgrading bitumen from oil sands. *Energy*, *36*(11), 6326-6339.

Oskay, C. (2014). Sürdürülebilir Kalkınma Çerçevesinde Rüzgar Enerjisinin Önemi Ve Türkiye'de Rüzgar Enerjisi Yatırımlarına Yönelik Teşvikler. *Niğde Üniversitesi İktisadi Ve İdari Bilimler Fakültesi Dergisi*, *7*(1), 76.

Ouyang, C., Wang, X., Wang, C., Zhang, X., Wu, J., Ma, Z., ... & Wang, S. (2015). Hierarchically porous Ni3S2 nanorod array foam as highly efficient electrocatalyst for hydrogen evolution reaction and oxygen evolution reaction. *Electrochimica Acta*, *174*, 297-301.

Panwar, N. L., Kaushik, S. C., & Kothari, S. (2011). Role of renewable energy sources in environmental protection: A review. *Renewable and sustainable energy reviews*, *15*(3), 1513-1524.

Peng, L., Shen, J., Zheng, X., Xiang, R., Deng, M., Mao, Z., ... & Wei, Z. (2019). Rationally design of monometallic NiO-Ni3S2/NF heteronanosheets as bifunctional electrocatalysts for overall water splitting. *Journal of Catalysis*, *369*, 345-351.

Peharz, G., Dimroth, F., & Wittstadt, U. (2007). Solar hydrogen production by water splitting with a conversion efficiency of 18%. *International Journal of Hydrogen Energy*, *32*(15), 3248-3252.

Rao, Y., Ning, H., Ma, X., Liu, Y., Wang, Y., Liu, H., ... & Wu, M. (2018). Template-free synthesis of coral-like nitrogen-doped carbon dots/Ni3S2/Ni foam composites as highly efficient electrodes for water splitting. *Carbon*, *129*, 335-341.

Ren, S., Duan, X., Ge, F., Zhang, M., & Zheng, H. (2020). Trimetal-based N-doped carbon nanotubes arrays on Ni foams as self-supported electrodes for hydrogen/oxygen evolution reactions and water splitting. *Journal of Power Sources*, *480*, 228866.

Safari, F., & Dincer, I. (2018). Assessment and optimization of an integrated wind power system for hydrogen and methane production. *Energy Conversion and Management*, *177*, 693-703.

Safari, F., & Dincer, I. (2020). A study on the Fe–Cl thermochemical water splitting cycle for hydrogen production. *International Journal of Hydrogen Energy*, *45*(38), 18867-18875.

Schnuelle, C., Wassermann, T., Fuhrlaender, D., & Zondervan, E. (2020). Dynamic hydrogen production from PV & wind direct electricity supply–Modeling and techno-economic assessment. *International Journal of Hydrogen Energy*, *45*(55), 29938-29952.

Şenel, M.Ç. & Koç, E. (2015). Dünyada Ve Türkiye'de Rüzgâr Enerjisi Durumu-Genel Değerlendirme . Mühendis Ve Makina , 56 (663) , 46-56.

Tao, L., Guo, P., Zhu, W., Li, T., Zhou, X., Fu, Y., ... & Ji, H. (2020). Highly efficient mixed-metal spinel cobaltite electrocatalysts for the oxygen evolution reaction. *Chinese Journal of Catalysis*, *41*(12), 1855-1863.

Temiz, M., & Javani, N. (2020). Design and analysis of a combined floating photovoltaic system for electricity and hydrogen production. *International Journal of Hydrogen Energy*, *45*(5), 3457-3469.

Tolstoy, V. P., Kuklo, L. I., & Gulina, L. B. (2019). Ni (II) doped FeOOH 2D nanocrystals, synthesized by Successive Ionic Layer Deposition, and their electrocatalytic properties during oxygen evolution reaction upon water splitting in the alkaline medium. *Journal of Alloys and Compounds*, *786*, 198-204.

Qazi, A., Hussain, F., Rahim, N. A., Hardaker, G., Alghazzawi, D., Shaban, K., & Haruna, K. (2019). Towards sustainable energy: a systematic review of renewable energy sources, technologies, and public opinions. *IEEE Access*, *7*, 63837-63851.

Qian, G., Mo, Y., Yu, C., Zhang, H., Yu, T., Luo, L., & Yin, S. (2020). Free-standing bimetallic CoNiTe2 nanosheets as efficient catalysts with high stability at large current density for oxygen evolution reaction. *Renewable Energy*, *162*, 2190-2196.

Vinodh, R., Deviprasath, C., Gopi, C. V. M., Kummara, V. G. R., Atchudan, R., Ahamad, T., & Yi, M. (2020). Novel 13X Zeolite/PANI electrocatalyst for hydrogen and oxygen evolution reaction. *International Journal of Hydrogen Energy*, *45*(53), 28337-28349.

Wang, Z., Wang, H., Ji, S., Wang, X., Pollet, B. G., & Wang, R. (2020). Multidimensional regulation of Ni3S2@ Co (OH) 2 catalyst with high performance for wind energy electrolytic water. *Journal of Power Sources*, *446*, 227348.

Winther-Jensen, B., & MacFarlane, D. R. (2011). New generation, metal-free electrocatalysts for fuel cells, solar cells and water splitting. *Energy & Environmental Science*, *4*(8), 2790-2798.

Wu, Y., Liu, Y., Li, G. D., Zou, X., Lian, X., Wang, D., ... & Zou, X. (2017). Efficient electrocatalysis of overall water splitting by ultrasmall NixCo3− xS4 coupled Ni3S2 nanosheet arrays. *Nano Energy*, *35*, 161-170.

Wu, C., Liu, B., Wang, J., Su, Y., Yan, H., Ng, C., ... & Wei, J. (2018). 3D structured Mo-doped Ni3S2 nanosheets as efficient dual-electrocatalyst for overall water splitting. *Applied Surface Science*, *441*, 1024-1033.

Xie, T., Zhao, H., Lv, Z., Xie, G., & He, Y. (2021). A highly active composite electrocatalyst Ni–Fe–P–Nb2O5/NF for overall water splitting. *International Journal of Hydrogen Energy*, *46*(1), 581-588.

Yadav, A. A., Hunge, Y. M., & Kang, S. W. (2021). Spongy ball-like copper oxide nanostructure modified by reduced graphene oxide for enhanced photocatalytic hydrogen production. *Materials Research Bulletin*, *133*, 111026.

Yadav, A. A., Hunge, Y. M., & Kang, S. W. (2021). Ultrasound assisted synthesis of highly active nanoflower-like CoMoS4 electrocatalyst for oxygen and hydrogen evolution reactions. *Ultrasonics Sonochemistry*, *72*, 105454.

Yıldız, R., Doğru Mert, B., Karazehir, T., Gurdal, Y., & Toprak Döşlü, S. (2021). Experimental and theoretical study on hydrogen production by using Ag nanoparticle-decorated graphite/Ni cathode. *International Journal of Energy Research*, *45*(3), 4068-4080.

Yoo, H., Kahng, S., & Kim, J. H. (2020). Z-scheme assisted ZnO/Cu2O-CuO photocatalysts t o increase photoactive electrons in hydrogen evolution by water splitting. *Solar Energy Mater ials and Solar Cells*, *204*, 110211.

Yıldız, R., Doğru Mert, B., Karazehir, T., Gurdal, Y., & Toprak Döşlü, S. (2021). Experimental and theoretical study on hydrogen production by using Ag nanoparticle-decorated graphite/Ni cathode. *International Journal of Energy Research*, *45*(3), 4068-4080.

Zhao, S., Wang, Q., Dong, S., Chen, J., & Wang, S. (2020). Phosphated NiCo2O4 nanoneedle arrays on flexible carbon filaments for effective oxygen evolution reaction in alkaline aqueous conditions: cooperation of small-sized effect and heteroatomic doping activation. *Chemical Engineering Journal*, *401*, 126156.

Zhang, Q., & Guan, J. (2020). Atomically dispersed catalysts for hydrogen/oxygen evolution reactions and overall water splitting. *Journal of Power Sources*, *471*, 228446.

Zhang, D., Jiang, L., Liu, Y., Qiu, L., Zhang, J., & Yuan, D. (2019). Ni3S2-MoSx nanorods grown on Ni foam as high-efficient electrocatalysts for overall water splitting. *International Journal of Hydrogen Energy*, *44*(33), 17900-17908.

Zhang O., Li F., Ji S., Yang J., Zhang C., Yang F., Lixu Lei. (2020). One-step electrodeposition of cauliflower-like Ni–Fe–Sn particles as a highly-efficient electrocatalyst for the hydrogen evolution reaction . *International Journal of Hydrogen Energy*.

Zhuang, S., Tong, S., Wang, H., Xiong, H., Gong, Y., Tang, Y., ... & Wan, P. (2019). The P/NiFe doped NiMoO4 micro-pillars arrays for highly active and durable hydrogen/oxygen evolution reaction towards overall water splitting. *International Journal of Hydrogen Energy*, *44*(45), 24546-24558.

Zhu, S., Lei, J., Zhang, L., & He, J. (2020). CoO/NF nanowires promote hydrogen and oxygen production for overall water splitting in alkaline media. *International Journal of Hydrogen Energy*, *45*(15), 8031-8040.

Zhu, J., Meng, X., & Xiao, F. (2013). Mesoporous zeolites as efficient catalysts for oil refining and natural gas conversion. *Frontiers of Chemical Science and Engineering*, *7*(2), 233-248.